Sapienza University of Rome
Faculty of Mathematical, Physical and Natural Sciences Department of
Biology and Biotechnology "Charles Darwin"

PhD Course in Cellular and Developmental Biology

Serpin function and disease: cellular toxicity of neuroserpin polymers and novel roles of alpha1-antitrypsin

PhD student

Emanuela D'Acunto

Supervisor

Prof. Maria Elena Miranda Banos

Coordinator

Prof. Giulia De Lorenzo

XXXII Cycle (2018/2019)

Alla mia famiglia,

Mamma Papà e Laura

INDEX

GENERAL INTRODUCTION

Serpins are the largest and most broadly distributed superfamily of protease inhibitors (Irving et al., 2000). Members of the serpin superfamily are found in all major branches of life including viruses, prokaryotes and eukaryotes. The serpin superfamily is characterised by more than 30% amino acid sequence homology with the archetypal serpin, antitrypsin (A1AT) (Carrell et al., 1985), a secretory serpin produced in the liver and delivered to the blood, through which it reaches the lungs where inhibits the protease neutrophil elastase. Serpins are mid-sized proteins (about 400 aminoacidic residues) whose tertiary structure consists of three β-sheets (A, B, and C), ten α-helices, and an exposed reactive center loop (RCL) of about 25 residues tethered between β-sheets A and C (Potempa et al., 1994) (Fig.1). This tertiary fold traps the molecule in a metastable conformation, resulting mainly from the labile configuration of a pair of parallel β-strands within the large central β sheet-A (strands s3A and s5A) (Gettins, 2002). Serpins are omnipresent throughout the body, residing both intra- and extra-cellularly. Circulating serpins are variably glycosylated, but the carbohydrate side chains are not required for inhibitory activity. Other inhibitory serpins are central in controlling proteolytic cascades in a number of fundamental biological pathways including blood coagulation, fibrinolysis, complement activation, and extracellular matrix (ECM) remodeling (such as neuroserpin). Inhibitory serpins are distinguished from all other protease inhibitors by their ability to set into motion a mousetrap-like mechanism that not only entraps the protease but also inactivates it.

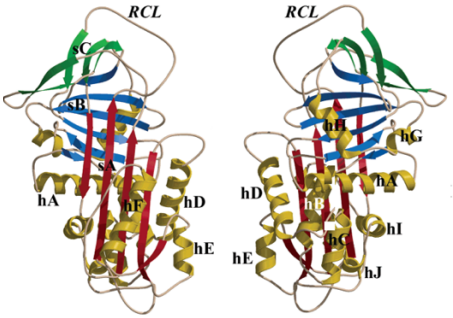

Figure 1. The secondary structural features of a serpin. β sheets A, B, and C are shown in red, blue and green, respectively. The ten α helices are designated A through H (hA – hH, all in yellow). The reactive center loop (RCL) is indicated in yellow at the top of the molecule. The first and second figure show respectively the front and the back of the protein. (Gettins, 2002).

The protease recognition site is contained within the exposed RCL in an accessible region for protease docking. Cleavage of the reactive site bond (termed the P1-P1' bond) by the protease triggers a dramatic change in the conformation of both the serpin and the protease. The N-terminal portion of the cleaved RCL inserts as the fourth strand into the gap between strands s3A and s5A to yield a fully antiparallel β-sheet A (Huntington 2000; Gettins 2002; Huntigton 2011). During this transition, termed the stressed to relaxed transition, the RCL transports the covalently linked protease (at its intermediate stage of the catalytic cycle) from one pole of the serpin molecule to the other. Although the overall shape of the serpin molecule is not altered by this transition, the resulting

conformation, in which the cleaved RCL is accommodated within β-sheet A, is much more stable than the conformation of the native molecule. Most of the energy released by this transformation is used to severely distort the structure of the protease, as evident from the resolved crystal structures of several serpin-protease complexes. A negative consequence of these requirements is that the inhibitory activity of serpins is susceptible to impairment by point mutations which may lead to both deficiency and degenerative disorders. Most serpin-related disorders are caused by point mutations that, alone or in combination with other factors, disrupt the delicate conformation of the mutated serpin, rendering it vulnerable to self-association and tissue deposition. Amino acid substitutions in serpins result in an aberrant conformational transition that causes a spectrum of pathologies knows as serpinopathies. The serpinopathies are protein conformational diseases characterised by the polymerisation and intracellular deposition of mutant variants of the serpins within the endoplasmic reticulum (ER) of the cells that synthesize the protein. Currently, three models of serpin polymerisation are proposed in the literature, differing in the number of β-strands (1, 2, or 3) involved in the intermolecular linkage (Lomas et al.,1992; Ekeowa et al., 2010; Yamasaki et al., 2008; Yamasaki et al., 2011) (Fig.2). However, all three models incorporate release of strand 1 of beta-sheet C, expansion of β-sheet A and insertion of reactive loop residues as an extra strand in beta-sheet A. The first model, proposed by Lomas and collaborators, suggests that the RCL is the only structural element inserted into the A sheet of an adjacent molecule during polymerisation (Lomas et al., 1992) [Fig. 2B(i)]. Yamasaki et al. have proposed an alternative linkage by the

crystal structures of a dimer of antithrombin in which the molecules were linked by a beta-hairpin of the RCL and strand 5A (Yamasaki et al., 2008) [Fig. 2B(ii)]. More recently, a triple-strand model of polymerisation was extrapolated from the crystal structure of a closed trimer of A1AT (Yamasaki et al., 2011) [Fig. 2B(iii)]. The intermolecular linkage consists of the three C-terminal ß-strands (strand 1 of ß-sheet C and strands 4 and 5 of ß-sheet B of AAT). This mechanism, as the second one, requires a substantially unfolded intermediate state, associated with intramolecular insertion of the reactive site loop. In general, the mutation causes a conformational transition and the formation of an unstable intermediate characterised by the "opening" of the βA sheet and the partial insertion of the RCL, which is no longer exposed to the solvent. The formation of polymeric chains causes, for each mutant serpin, a loss-of-function phenotype due to the lack of active serpin in the extracellular place of action, and in some cases a gain-of-toxic-function phenotype due to intracellular polymer accumulation in the tissue of synthesis.

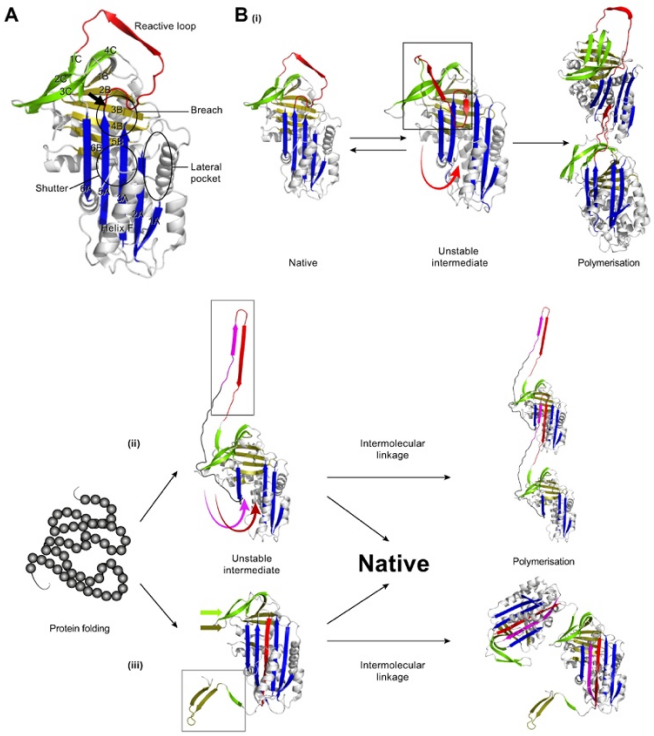

Figure 2. Models of A1AT polymerisation. A. Crystal structure of native A1AT and key features indicated. The reactive loop (red), beta-sheet A in blue, beta-sheet B in gold, and beta-sheet C in green. The arrow indicates the site of the Z mutation, within the breach region where initial intramolecular loop insertion may occur. **B.** Three models of polymerisation. (i) Single strand (reactive loop) linkage model; (ii) beta-hairpin (strands 5A + 6A) linkage model; (iii) triple-strand (C-terminal motif: beta-strands 1C, 4B + 5B) linkage model (Lomas et al., 2016).

AIMS OF THE WORK

Serpinopathies are characterised by the misfolding and intracellular polymerisation of mutant forms of the serpin within the ER of the cell of synthesis and can be classified as "conformational diseases" that arise when proteins undergo self-association and tissue deposition (Carrell and Lomas, 1997). The retention of mutant protein causes damage due to the presence of polymers in the cell that synthetize the protein, whilst the lack of the circulating protease inhibitor causes an ineffective inhibition of its specific target (Lomas et al., 2016). These problems predispose the individuals to develop severe diseases depending on the type of mutated serpin. Examples of human mutant serpins accumulating and causing a toxic gain of function are alpha 1-antitrypsin (A1AT) variants causing cirrhosis (Sharp et al., 1969) and mutants of neuroserpin (NS) causing the dementia familial encephalopathy with NS inclusion bodies (FENIB) (Davis et al., 1999a). The best characterised of the serpinopathies is surely A1AT deficiency in which the Z mutation causes the retention of protein within hepatocytes, giving rise to inclusion bodies, in association with neonatal hepatitis, cirrhosis and hepatocellular carcinoma (Sveger et al., 1976; Dawwas et al., 2013), whilst the lack of A1AT, an important lung elastase inhibitor, predisposes the Z homozygote to early onset panlobular basal emphysema (Eriksson et al., 1986). FENIB is an autosomal dominantly inherited disease characterised clinically as a spectrum of phenotypes, from dementia to epilepsy with variable electrical status (Gooptu et al., 2009), with the presence of eosinophilic neuronal inclusions distributed throughout the deeper layers of the cerebral cortex and in many subcortical nuclei, especially

the *substantia nigra*. To date, six different mutations have been described in NS that promote its polymerisation in people affected by FENIB. In this work our interest is to evaluate with diverse approaches very different aspects of both pathologies. In the case of NS, following previous work in our laboratory in which we demonstrated the presence of oxidative stress in a novel neuronal model for FENIB neurodegeneration (Guadagno et al., 2017), our interest is to evaluate the cellular aspects involved in the polymer toxicity, focusing in particular on the mitochondrial network and its interconnection with oxidative stress and ER disfunctions. For A1AT deficiency, our interest is to explore a non-inhibitory function of this protein, to date not well understood and apparently not directly related with the onset of the pathology: its immunomodulatory role.

SECTION I

MUTANT NEUROSERPIN INDUCES MITOCHONDRIAL ALTERATIONS IN A NEURONAL MODEL OF DEMENTIA FENIB

SUMMARY

Neuroserpin (NS) is a protein belonging to the serpins (serin protease inhibitors), a conserved superfamily of proteins that inhibit serin proteases. Several mutations have been identified as the cause of different pathologies, where mutant serpins form chains of polymers that accumulate within the endoplasmic reticulum (ER) of the cell of synthesis. The neurodegenerative dementia FENIB (familiar encephalopathy with neuroserpin inclusion bodies) is caused by polymerisation and deposition of the neuronal serpin neuroserpin within the ER of neurons. With the aim of understanding the toxicity due to intracellular accumulation of NS polymers, we have generated transgenic neural stem progenitor cells (NSPCs) from mouse fetal cerebral cortex, stably expressing the control protein GFP (green fluorescent protein), or human wild type (WT), polymerogenic G392E (GE) or truncated (delta) NS. In this cellular model, we have described the upregulation of several genes involved in the defense against oxidative stress in cells expressing G392E NS (*Aldh1, Apoe, Gpx1, Gstm1, Prdx6, Scara3, Sod2)* (Guadagno et al., 2017). We are now investigating the involvement of mitochondria in NS polymer toxicity. Our analysis of mitochondrial distribution shows a perinuclear redistribution of these organelles in G392E NS

cells, in contrast with filamentous mitochondria in cells expressing wild type NS or GFP. This phenotype is aggravated to mitochondrial fragmentation in the presence of a glutathione chelator, supporting a link between oxidative stress and mitochondrial dysfunction in the neurodegeneration FENIB. Moreover, treatment with the antioxidant molecules melatonin and tocopherol improves the perinuclear phenotype of the G392E NS cells, back to a distribution comparable to that of control cells. We also investigated the cellular morphology looking at the actin cytoskeleton and our results show an altered cellular morphology in cells that have altered mitochondria, in particular G392E NS cells show a lower number of well-developed neurites compared to WT NS cells. We evaluated mitochondrial function and found that the potential of the inner mitochondrial membrane is lower in G392E than WT NS cells, but no other parameters of the mitochondrial metabolism seemed to be altered as per seahorse analysis of the total population of cells. Lastly, in order to better understand how NS polymers cause mitochondrial deregulation, we evaluated the ER-mitochondria contact regions and found that in G392E NS cells these are less abundant than in cells expressing wild type NS.

SOMMARIO

La neuroserpina (NS) è una proteina facente parte delle serpine (inibitori di serin proteasi), una superfamiglia di proteine altamente conservata che inibisce le proteasi a serina. Fino ad ora sono state identificate numerose mutazioni alla base di altrettante patologie, dove le serpine mutanti formano

catene di polimeri che si accumulano nel reticolo endoplasmatico (RE) della cellula di sintesi. La neurodegenerazione FENIB (encefalopatia familiare con corpi di inclusione di neuroserpina) è causata dalla polimerizzazione e deposizione della serpina neuronale NS nel RE dei neuroni. Con il fine di comprendere la tossicità causata dall'accumulo intracellulare dei polimeri di NS, sono state generate linee di cellule staminali progenitrici neurali transgeniche, derivate dalla corteccia cerebrale fetale di topo ed esprimenti stabilmente la proteina di controllo GFP, o la NS umana in versione *wild type* (WT), la forma polimerogenica G392E (GE) o la variante troncata (delta) NS. In questo modello cellulare abbiamo già descritto l'aumento d'espressione di numerosi geni coinvolti nella difesa contro lo stress ossidativo nelle cellule che esprimono G392E NS (*Aldh1, Apoe, Gpx1, Gstm1, Prdx6, Scara3, Sod2)* (Guadagno et al., 2017). I nostri studi mirano attualmente a comprendere il coinvolgimento dei mitocondri nella tossicità indotta dai polimeri di NS. Le nostre analisi sulla distribuzione mitocondriale mostrano una redistribuzione perinucleare di questi organelli nelle cellule G392E, in contrasto con mitocondri disposti in maniera filamentosa delle cellule esprimenti neuroserpina WT o GFP. Questo fenotipo viene esacerbato fino alla frammentazione mitocondriale in presenza di un chelante del glutatione, il che supporta un collegamento tra stress ossidativo e il fenotipo mitocondriale presente nella demenza FENIB. All'opposto, il trattamento con le molecole antiossidanti tocoferolo e melatonina migliora il fenotipo perinucleare delle cellule G392E fino a valori comparabili ai controlli. Abbiamo inoltre studiato la morfologia cellulare concentrandoci sul citoscheletro actinico e i nostri risultati mostrano una alterata

morfologia cellulare nei neuroni che presentano una alterata distribuzione mitocondriale; nel concreto, le cellule G392E NS hanno un numero minore di neuriti ben sviluppati quando comparate con le cellule WT. Abbiamo anche valutato la funzione mitocondriale e abbiamo trovato che il potenziale della membrana mitocondriale interna è minore nelle cellule G392E NS rispetto alle WT, ma nessun altro parametro del metabolismo mitocondriale sembra essere deregolato se valutati tramite *seahorse assay* sulla popolazione cellulare totale. Infine, con l'obiettivo di comprende meglio come i polimeri di NS influiscono sulla deregolazione mitocondriale, abbiamo valutato le aree di contatto tra RE e mitocondri, trovando che nelle cellule G392E NS ci sono meno punti di contatto tra i due organelli.

Introduction

The serpinopathies are protein conformational diseases characterised by the polymerisation and intracellular deposition of mutant variants of the serpins, within the endoplasmic reticulum (ER) of the cells that synthesize the protein. This mechanism results, in our case, in a neuropathological condition caused by mutations in neuroserpin (NS) (Roussel et al., 2011). This pathology, an autosomal dominant condition known as FENIB (familial encephalopathy with neuroserpin inclusion bodies), is a neurodegenerative dementia (Davis et al., 1999a). To date, six different mutations have been described in NS that promote its polymerisation in people affected by FENIB: Ser49Pro (*Syracuse*), Ser52Arg (*Portland*), His338Arg, Gly392Glu, Gly392Arg and Leu47Pro. Mutant NS was found to accumulate within affected neurons forming periodic acid-Schiff (PAS)-positive inclusion bodies known as Collins bodies, most abundant in the cerebral cortex but also present in other regions of the central nervous system (Davis et al., 1999b). Clinically this accumulation is translated in a spectrum of phenotypes, from dementia to epilepsy with variable electrical status (Roussel et al., 2016). These main phenotypical and biochemical features of FENIB deduced, respectively, from its clinical manifestations and from the postmortem analysis of affected brains, were confirmed through the expression of mutant NS in mice (Madani et al., 2003; Galliciotti et al., 2007), in *Drosophila melanogaster* (Miranda et al., 2008) and in diverse cellular systems (Miranda et al., 2004, 2008; Roussel et al., 2013). Transgenic mice overexpressing S49P and S52R NS showed the formation of

abundant intraneuronal Collins bodies, neuronal loss in the cerebral cortex and hippocampus, and pathological phenotypes reminiscent of FENIB during late adulthood, while overexpression of human S49P, S52R, H338R and G392E NS in *Drosophila melanogaster* led to a decrease in locomotor activity, with decreasing mobility correlating to increased polymer content in the brain. In cellular models, polymer formation and its correlation with the disease phenotype was confirmed in transiently transfected COS-7 and stable inducible PC12 cell models of FENIB, where overexpression of each mutant variant lead to intracellular accumulation of polymeric NS within the ER to a degree that was proportional to the severity of FENIB as seen in patients (Miranda et al., 2004, 2008; Moriconi et al., 2015). Despite these results, the mechanism of toxicity of NS polymers in cellular models of disease has been elusive so far, since these cellular systems failed to show clear signs of cell malfunction and death upon NS polymer accumulation, precluding a detailed investigation of the mechanisms underlying NS polymer toxicity. This lack of a toxic phenotype could be related to the proliferative nature of these cell lines. To overcome these issues, we have recently developed a neuronal model with stable overexpression of WT, G392E and delta NS. Mouse neural stem cell progenitors were isolated from the cortex of mouse foetal brain, transfected with the NS variants and propagated *in vitro* as proliferative cells, and later differentiated to mature, non-dividing neurons for detailed studies of polymer toxicity. Our group has recently shown that, in this cellular model, expression of mutant G392E NS causes oxidative stress (Guadagno et al., 2017).

Oxidative stress, the imbalance between generation and disposal of reactive oxygen species (ROS), is an important factor in several neurodegenerative disorders including Alzheimer's, Parkinson's and Huntington's diseases and amyotrophic lateral sclerosis (Cobb and Cole, 2015). Neurons are particularly vulnerable to oxidative stress due to their high energy requirements, to a decrease in antioxidant defenses with age and to their terminally differentiated nature, and so oxidative stress is a key player in neurodegenerative disorders (Gandhi and Abramov, 2012). Under physiological conditions, ROS have important roles in signaling and immune defense, and their levels are kept under check by several antioxidant defense systems, including enzymatic (mainly superoxide dismutase, glutathione peroxidase, catalase and thioredoxin reductase) and non-enzymatic (specially glutathione, GSH) mechanisms, which can either scavenge ROS or decrease their formation (Li et al., 2013). The ER, where NS polymer formation takes place, provides an oxidizing environment for correct formation of disulfide bonds during protein folding. Accumulating evidence suggests that ROS can be generated as a by-product of protein oxidation during normal ER function and also upon ER stress due to accumulation of misfolded proteins. Both ER stress and oxidative stress, through ROS generation, may increase the leak of Ca^{2+} from the ER lumen, as well as induce protein and lipid oxidation. All these evidences support that the accumulation of serpin polymers within the ER may upset the redox balance in this organelle.

The importance of mitochondria in energy production has long been appreciated, but new research into the dynamic nature of mitochondria has highlighted their role in normal cell

physiology and disease (Knott et al., 2008). Mitochondria are important organelles in all cell types, but they are particularly important in the nervous system. Mitochondrial function is essential to neuronal processes such as energy production, Ca^{2+} regulation, maintenance of plasma membrane potential, protein folding by chaperones, axonal and dendritic transport and the release and re-uptake of neurotransmitters at synapses (Hoppins et al., 2007; Zhang et al., 2007). Because mitochondria are the main source of ROS, oxidative damage of mitochondrial proteins or DNA is likely to contribute to the mitochondrial dysfunction that is characteristic of many neurodegenerative disorders (Lin et al., 2006). High levels of ROS generation within the mitochondria further increase Ca^{2+} release from the ER, generating a vicious cycle of ROS production and cellular oxidative stress (Malhotra and Kaufman, 2007). From this starting point, in this work we decided to focus on mitochondrial behavior in our cell lines to better understand the interconnection between NS polymer, oxidative stress and neuronal toxicity.

Results

Generation and characterization of NSPCs expressing NS

Since the cell lines in use can only be amplified for a limited number of passages, we decided to produce again the neural stem progenitor cell (NSPC) lines starting from murine cortex cells at 13.5 days of embryonic development (E13.5), as described in Guadagno et al. (2017). In order to gain a better knowledge of our cell model system, we assessed the levels of endogenous NS in *naïve* (non-transfected) NSPCs in proliferative conditions *versus* cells differentiated to a neuronal phenotype following our *in vitro* differentiation protocol for six days (Soldati et al., 2012). By real-time RT-PCR, we found that endogenous mouse NS expression increased approximately five times upon differentiation of NSPCs into neurons, and that expression levels in differentiated cells were nearly 30% of those found in E13.5 mouse telencephalic tissue (Fig. 1A, left panel). As a control, the expression of *Dcx*, a marker for differentiating neuroblasts, was strongly increased following six days of culture in differentiating conditions (Fig. 1A, right panel). Furthermore, to evaluate the differentiating conditions used for our assays, we performed an immunofluorescence for the neuronal marker β III tubulin and counted the positive cells on the total population, finding a percentage of nearly 55-60% of neurons (Fig. 1B).

A

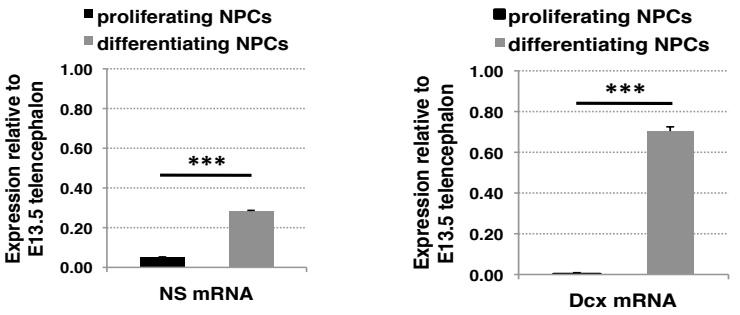

B

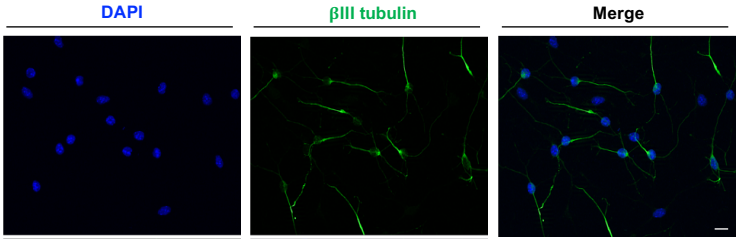

Figure 1. Characterization of NS expression in *naïve* cells and differentiating conditions. A. *Naïve* cell expression of endogenous NS mRNA in proliferating and differentiating conditions compared to expression in E13.5 telencephalon (left), and expression of the positive control gene for neuroblast differentiation *Dcx* (right). n=3 Data are mean ± SEM, t-test: ***p ≤ 0.001. **B.** Immunofluorescence for βIII tubulin (green) to evaluate the number of neurons on the total cell population after

six days treatment with the differentiation protocol. Cell nuclei were stained with DAPI (blue) Scale bar 10μm.

As described in Guadagno et al. (2017), we introduced the transgenes by electroporation for constitutive expression of GFP and the NS variants. We thus recreated the four transgenic cell lines, which permanently overexpressed wild type NS (WT NS), the strongly polymerogenic G392E NS (GE NS), the truncated protein delta NS (dNS) and the green fluorescent protein (GFP), respectively. In all plasmids, the sequence for the gene of interest (NS or GFP) and the one for the puromycin resistance gene are expressed in a single bicistronic mRNA via an internal ribosome entry site (IRES), under the control of a strong CAG promoter that contains the enhancer sequence of human cytomegalovirus (CMV), which promotes constitutive expression of the gene of interest (Vallier et al., 2005) (Fig. 2A). NSPCs with stable integration and expression of WT, G392E NS, dNS or control GFP were selected and maintained by culturing in the presence of 1 μg/ml puromycin. We verified the correct expression of these constructs in our transgenic NSPC differentiated cultures by SDS and by non-denaturing PAGE followed by western blot analysis of the cell lysates and culture media (Fig. 2B). The results show that in denaturing conditions WT NS was found as a single band of nearly 50 kDa, partially in the cell lysate and partially in the extracellular medium, showing that WT NS was normally processed and secreted as a monomer. In contrast, G392E NS was detected in the cell lysate as a doublet of two close bands and no signal was apparent in the medium. Delta NS was detectable only in cell lysates after proteasomal block with the MG132 inhibitor. When the same samples were

analyzed by non-denaturing PAGE and western blot, WT NS presented as a monomer, particularly visible in the culture medium, while G392E NS was detected as polymers of different sizes both in the cell lysate and culture medium. No NS signal was seen in the samples from GFP expressing cells that were used as negative control.

A

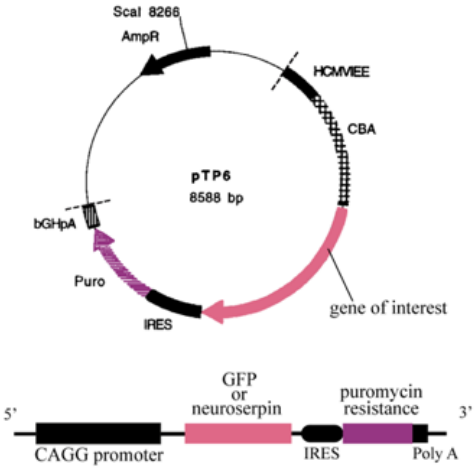

B

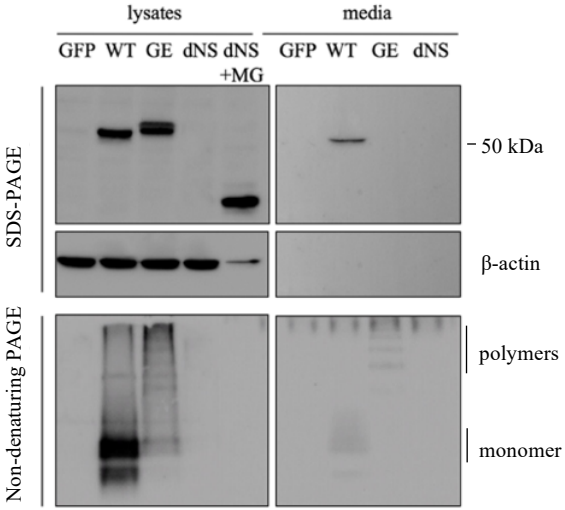

Figure 2. Expression of NS in NSPC. A. Schematic diagram of the pTP6 plasmid. The gene of interest and the puromycin resistance genes are separated by an internal ribosome entry site (IRES), and expression of both is driven by a human cytomegalovirus immediate early enhancer (HCMVIEE) coupled to the chicken β-actin promoter and first intron (CBA). The 3' end contains a bovine growth hormone polyadenylation signal (bGHpA). The plasmid was linearized with *Sca*I, which cut within the ampicillin resistance (ampR gene) prior to introduction into NPCs by electroporation. **B.** Cell lysates and culture media of stably transfected NSPCs after differentiation into neurons, expressing control GFP or WT, G392E NS or delta NS. The last line was treated

or not with the reversible proteasomal inhibitor MG132 (2 μM for 12h), but only the non-treated culture medium was collected, since this variant of NS is not secreted (Davies et al., 2009). Samples were resolved by 10% w/v acrylamide SDS and 7,5% w/v acrylamide non-denaturating PAGE, and analysed by western blot with an anti-neuroserpin polyclonal antibody. The same membrane was probed for the housekeeping enzyme beta actin as a loading control.

G392E NS expressing cells show altered mitochondrial distribution

Recent research has demonstrated the role of oxidative stress in neurodegenerative diseases and the importance of the communication between the ER (where mutated NS accumulates) and mitochondria, which is known to be the major organelle involved in the response to oxidative stress and the main intracellular source of ROS (Maharjan et al., 2014). We thus decided to look at the mitochondrial network in our cell lines. We stained the cells with Mitotracker Red CMXRos © (Mitotracker), which is a red fluorescent dye that labels mitochondria within living cells using the mitochondrial membrane potential. Based on the literature and on our analysis of the cellular phenotypes, we defined three categories of mitochondrial distribution (Fig. 3A): i) network mitochondria homogeneously distributed throughout the cytoplasm, forming a filamentous network within the neurons (left panel); ii) perinuclear: mitochondria that appeared clustered in the neuronal soma and generally on one side of the nucleus (middle panel); and iii) fragmented: mitochondria appeared as small and rounded, and located close to the nucleus (right panel). In our analysis, we grouped perinuclear and fragmented mitochondria as "altered" distribution. In basal conditions, WT and delta NS expressing cells mostly showed the network-like distribution, indicative of a healthy mitochondrial network. Cells expressing G392E NS showed a higher proportion of altered mitochondria (nearly 40%), which were often found clustered close to the nucleus with no mitochondrial fragmentation, indicative of the underlying toxicity caused by NS polymers. As shown in figure 3B,

neuronal exposure to the oxidative insult caused by H_2O_2 resulted in a significant change in mitochondrial distribution of control GFP cells: in untreated cells, healthy mitochondria were organized in a filamentous network; after exposure to H_2O_2 this transformed into a clustered distribution and in some cells into a fragmented phenotype. These changes resulted in a significant shift of mitochondria from category (i) into categories (ii) and (iii).

A

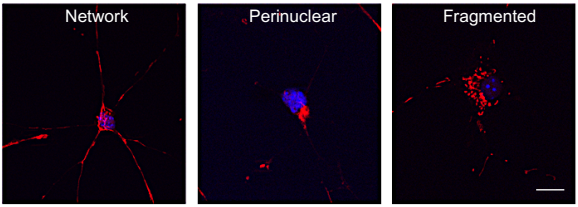

B

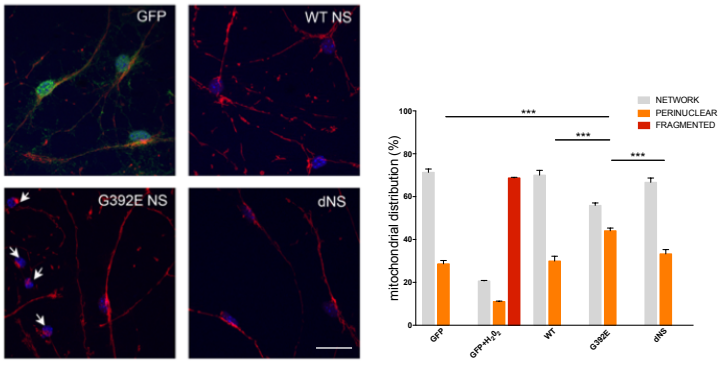

Figure 3. Analysis of mitochondrial distribution in differentiated NSPCs. A. NSPCs were differentiated for 6 days and mitochondrial distribution was characterised after staining with Mitotracker (red). Three different mitochondrial phenotypes were defined: network (left panel), which showed filamentous mitochondria distributed throughout the cells; perinuclear (middle panel), in which mitochondria were clustered close to the nucleus and typically on one side of it; and fragmented (right panel), characterised by the strongly punctuate staining around the nucleus. **B.** Immunofluorescence panel of the four cell lines evaluated and percentage of healthy (network) and altered (perinuclear + fragmented) mitochondria for each cell line. As a positive control, GFP cells were treated with H_2O_2 100 μM, which mostly induced mitochondrial fragmentation. Cell nuclei were stained with DAPI (blue). Data are mean ± SEM, n = 5; t-test: ***p ≤ 0.001. (n= 100 cells/ 5 independent experiments) Scale bar 10μm.

Alterations of the mitochondrial network are directly related to the presence of intracellular polymers

Since we have observed the presence of NS polymers in the culture medium of G392E NS cells by western blot, we quantified them by sandwich ELISA using a monoclonal antibody with higher affinity for polymeric than monomeric NS (7C6, Miranda et al., 2008), and found an average concentration of 1,25 ng/ml. To understand if the alterations in

the mitochondrial network of G392E NS cells is caused by the accumulation of polymers in the ER or to their presence in the culture medium, we treated GFP control cells with culture medium preconditioned by GFP cells or cells expressing WT or G392E NS. We collected the conditioned media after three days of differentiation and used them to treat GFP cells for another three days of differentiation. At the end of the treatment, we used Mitotracker to evaluate mitochondrial distribution (Fig.4) and found that there were no significant changes when treating GFP cells with medium conditioned by either WT or G392E NS cells.

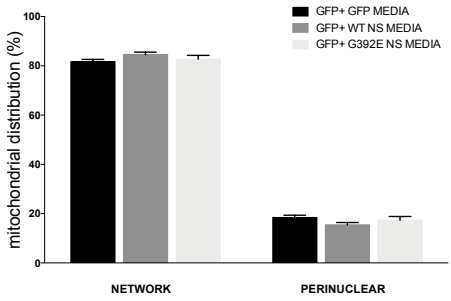

Figure 4. Analysis of mitochondrial distribution in GFP cells treated with preconditioned media derived from GFP, WT NS and G392E NS cells. GFP, WT NS and G392E NS cells were differentiated for 3 days, after which culture media were collected and used to treat GFP cells for the remaining 3 days of differentiation.

Mitochondrial distribution was assessed after staining with Mitotracker. There were no significant changes in mitochondrial distribution. Data are mean ± SEM, n = 5. (n= 100 cells/ 5 independent experiments).

Pharmacological inhibition of the antioxidant defenses leads to enhanced mitochondrial perturbation in G392E NS cells

We next decided to investigate the effect of pharmacological inhibition of the cellular defenses against oxidative stress. Glutathione (GSH) is an important antioxidant metabolite that prevents cell damage caused by the presence of ROS, lipid oxidases and free radicals, and is involved in the mechanism of action of several of the enzymes that were overexpressed in our G392E NS expressing cells. Cellular levels of GSH can be depleted by treating the cells with DEM (diethyl maleate). We stained the cells with Mitotracker after treating them with DEM 50 μM for 1h. As shown in figure 5, GFP, WT and delta NS expressing cells showed little alterations of mitochondrial distribution after DEM treatment, while cells expressing G392E NS showed a stronger response to the pro-oxidant treatment with DEM, with a significant increase in the number of cells showing fragmented distribution, thereby supporting the oxidative nature of the insult caused by the presence of G392E NS polymers in the ER.

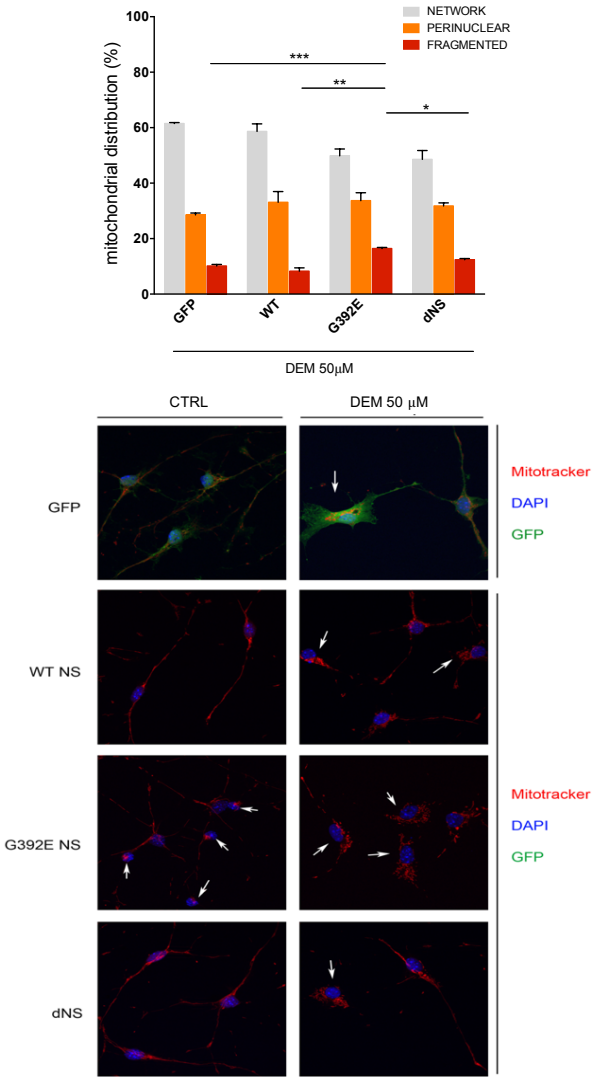
NETWORK
PERINUCLEAR
FRAGMENTED
mitochondrial distribution (%)
100
80
60
40
20
0
***
**
*
GFP
WT
G392E
dNS
DEM 50μM
CTRL
DEM 50 μM
GFP
WT NS
G392E NS
dNS
Mitotracker
DAPI
GFP
Mitotracker
DAPI
GFP

Figure 5. Analysis of mitochondrial distribution in differentiated NSPCs after DEM treatment. The percentage of healthy (network) and altered (perinuclear + fragmented) mitochondrial distribution was evaluated for each cell line after differentiation for 6 days and treatment with DEM at final concentration of 50 μM for 1h, by staining with Mitotracker and counting the cells with each of the three different distributions under a fluorescence microscope. Cell nuclei were stained with DAPI (blue). The graph shows the mean ± SEM, n = 3; t-test: ***p ≤ 0.001, **p ≤ 0.01, * p ≤ 0.05. (n= 100 cells/ 3 independent experiments) Scale bar 10μm.

The mitochondrial phenotype caused by expression of G392E NS is rescued by antioxidant molecules

We next decided to verify if antioxidant treatments could revert the perinuclear mitochondrial distribution seen in G392E NS cells. We selected two different antioxidants to test in our cell cultures: melatonin and alpha tocopherol. Melatonin is a pineal gland neurohormone that mediates photoperiodicity in mammals, and alpha tocopherol is a vitamin that function as a lipid soluble antioxidant protecting cell membranes from oxidative damage, but both are also well characterised antioxidant molecules. We first evaluated their effect in WT and G392E NS cells by treating them with increasing concentrations of melatonin and tocopherol for 24 and 48 h followed by staining with Mitotracker, to obtain dose-response curves for both molecules (Fig. 6A and B). After determining

the optimal concentration and time conditions, we treated all four cell lines with 10 μM of each of the two compounds for the lasts 48 h of differentiation. As shown in figures 7A and 7B, cells expressing GFP, WT and delta NS showed very mild changes, while cells expressing G392E NS showed a reduction in the percentage of cells with perinuclear distribution, decreasing to values similar to those seen for control cells.

A

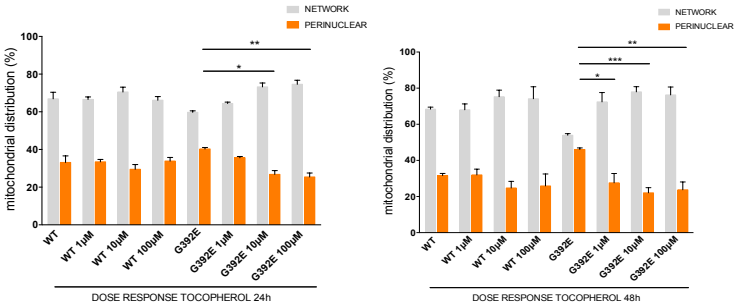

B

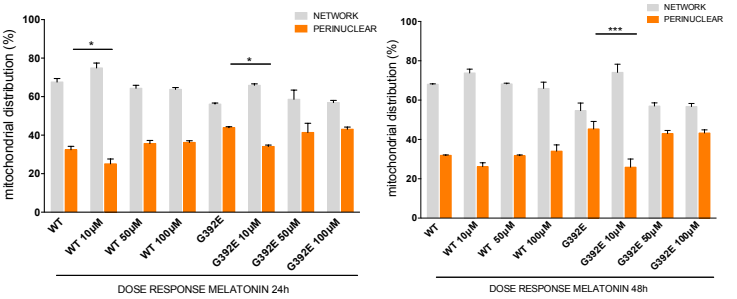

Figure 6. Dose-response curves for tocopherol and melatonin treatments. WT and G392E NS NSPCs were differentiated for 6 days and mitochondrial distribution was analyzed by staining with Mitotracker after treatment with tocopherol (**A**) or melatonin (**B**) at the indicated doses (1, 10, 100 μM) during the last 48 or 24 h of differentiation. Data are mean ± SEM, n = 3; t-test: ***p ≤ 0.001, **p ≤ 0.01, *p ≤ 0.05. (n= 100 cells/ 3 independent experiments).

A

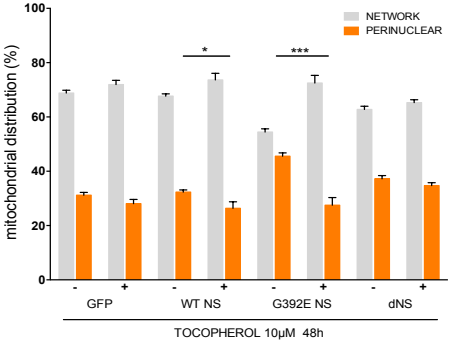
NETWORK
PERINUCLEAR
mitochondrial distribution (%)
100
80
60
40
20
0
*
***
-
+
GFP
WT NS
G392E NS
dNS
TOCOPHEROL 10μM 48h

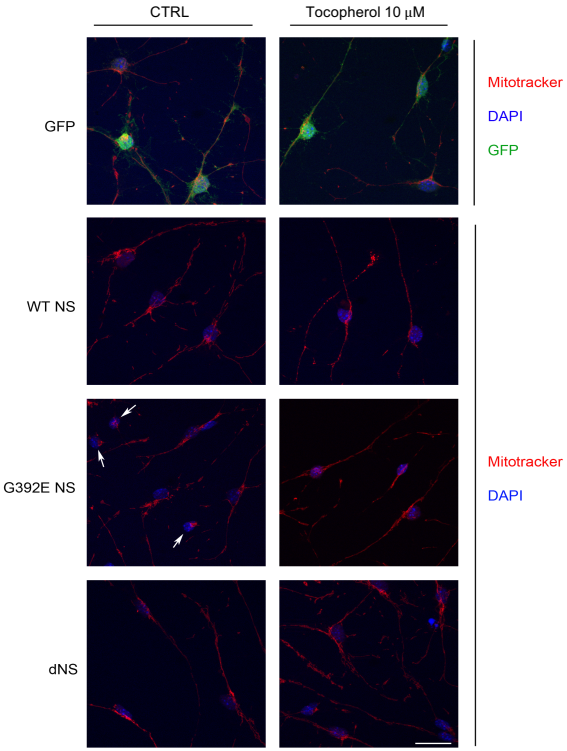
CTRL
Tocopherol 10 μM
GFP
WT NS
G392E NS
dNS
Mitotracker
DAPI
GFP
Mitotracker
DAPI

B

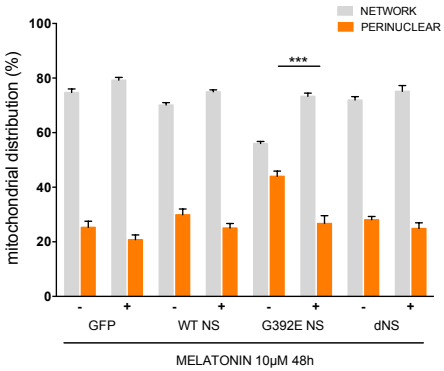
NETWORK
PERINUCLEAR
mitochondrial distribution (%)
100
80
60
40
20
0
***
- + - + - + - +
GFP
WT NS
G392E NS
dNS
MELATONIN 10μM 48h

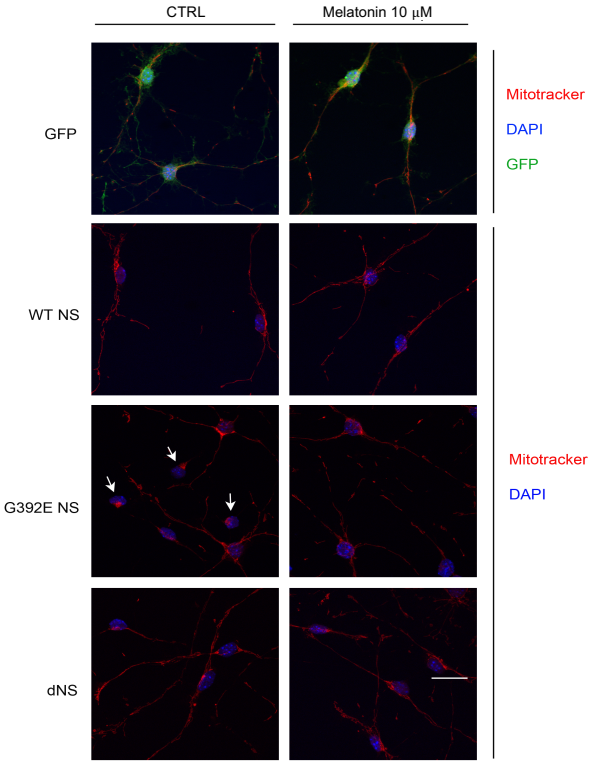
CTRL
Melatonin 10 μM
GFP
WT NS
G392E NS
dNS
Mitotracker
DAPI
GFP
Mitotracker
DAPI

Figure 7. Analysis of mitochondrial distribution in differentiated NSPCs treated with antioxidant molecules. NSPCs overexpressing GFP, WT NS, G392E NS or delta NS were differentiated for 6 days, treating with 10 μM alpha tocopherol (**A**) **or** 10 μM melatonin (**B**) during the last 48 h, and mitochondrial distribution was characterised by staining with Mitotracker. Cell nuclei were stained with DAPI (blue). Data are mean ± SEM, n = 5; t-test: ***p ≤ 0.001, * p ≤ 0.05. (n= 100 cells/ 5 independent experiments) Scale bar 10μm.

Cellular morphology is altered in cells with altered mitochondrial distribution

Given the altered distribution of mitochondria in our cells, we investigated if the general morphology of these cells was also altered, by looking at the actin cytoskeleton. We performed a double staining with Mitotracker and phalloidin-Alexa 488, which specifically binds the polymerised actin cytoskeleton, in cells differentiated for six days. Our results show a strong change in the morphology of cells that have perinuclear and fragmented mitochondrial phenotypes (Fig. 8). Neuronal cells that presented network mitochondrial distribution had well-developed neurites, while cells with a perinuclear or fragmented phenotype mitochondria located close to the

nucleus in correlation with the absence of well-developed neurites.

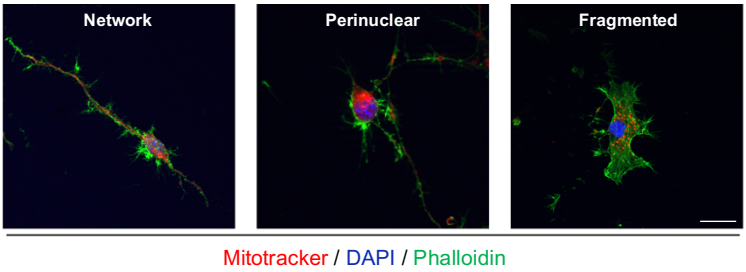

Figure 8. Neuronal morphology and mitochondrial distribution of differentiated NSPCs. NSPCs were differentiated for 6 days and double stained for mitochondrial morphology with Mitotracker and for cell morphology with phalloidin-Alexa 488 (red and green respectively). Cell nuclei were stained with DAPI (blue). Representative images obtained with a confocal microscope (Zeiss) Scale bar 10μm.

To quantify this observation, we evaluated neurite length in WT and G392E NS cells differentiated for six days and double stained with Mitotracker and phalloidin-Alexa 488, and measured neurite length using the image analysis software "Image J" (NIH software), a public domain Java image processing program, and the specific plug in "Neuron J". As

shown in figure 9, G392E NS cells had shorter neurites when compared to WT NS cells.

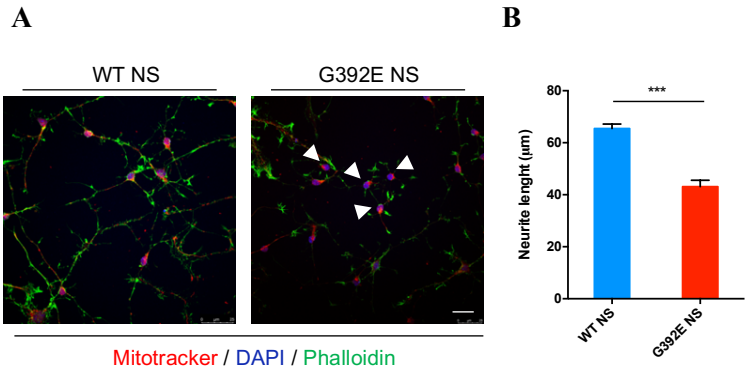

Figure 9. Evaluation of neurite length in differentiated NSPCs. A. NSPCs were differentiated for 6 days and mitochondrial morphology was assessed with Mitotracker and the cell morphology with phalloidin-Alexa 488 (red and green fluorescence respectively). Cell nuclei were stained with DAPI (blue). **B.** Quantification of neurite length in images obtained as in A, data are mean ± SEM, n=3; t-test: ***p ≤ 0.001. (n= 50 cells/ 3 independent experiments) Scale bar 10µm.

The potential of the inner mitochondrial membrane is lower in G392E NS than WT NS cells

To understand if the altered distribution of mitochondria is also related with functional alterations, we evaluated one of the most important parameters directly related to the health of mitochondria, the inner membrane potential. In order to asses this we used the cationic dye 5,5',6,6'-tetrachloro-1,1'3,3'-tetraethylbenzamidazol-carboncyanine (JC-1). Healthy mitochondria can transport JC-1 into their matrix, where it forms aggregates that produce red fluorescence. If the inner mitochondrial membrane is depolarized, the dye fails to cross it and remains outside the organelle in its monomeric form returning green fluorescence. The ratio between red and green fluorescence thus correlates with the potential of the inner mitochondrial membrane, allowing to assess mitochondrial state. Red JC-1 aggregates and green monomers were visualized simultaneously with a dual band-pass filter for fluorescein (Ex/Em 490/520 nm)/rhodamine (Ex/Em 540/570 nm). Confocal microscopy images of living cells were analyzed and quantitated as red (aggregate)/green (monomer) ratio using image analysis software “Image J”. As shown in figure 10, the proportion of green fluorescence in G392E NS cells is higher than in the WT NS ones, suggesting a functional alteration in mitochondria of cells expressing polymerogenic G392E NS.

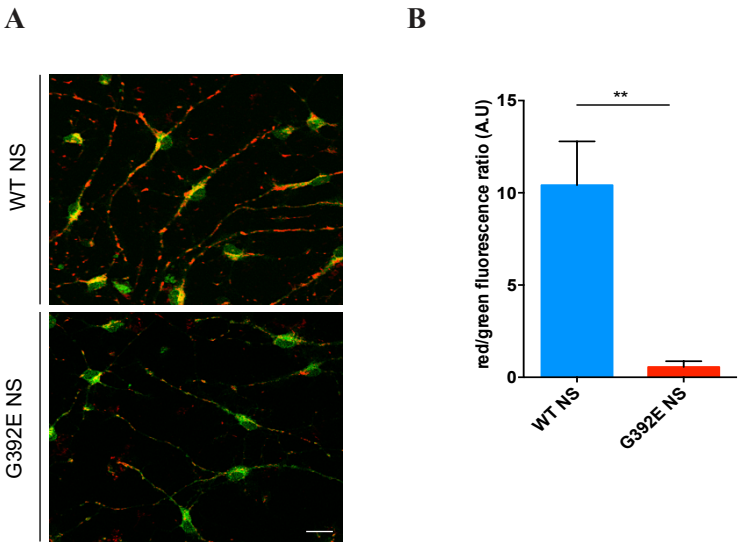

Figure 10. Evaluation of inner mitochondrial membrane potential using JC-1 staining in differentiated NSPCs. A. NSPCs were differentiated for 6 days and inner mitochondrial membrane potential was analyzed with the JC-1 probe by imaging of living cells with confocal microscopy. **B.** Quantification of the red fluorescence (aggregated JC-1)/green fluorescence (monomeric JC-1), mean ± SEM, n=3; t-test: **p ≤ 0.01. (n= 100 cells/ 3 independent experiments) Scale bar 10μm.

G392E NS cell cultures do not show alterations in mitochondrial metabolism

Mitochondria are essential for the energy metabolism of cells and alterations of the mitochondrial respiration can induce mitochondrial failure. Oxygen consumption rate (OCR) is an important indicator of normal cellular function and it is routinely used to investigate mitochondrial functionality. Using a Seahorse platform in collaboration with Prof. Michael Duchen (UCL, London, UK) and Lorita Gianfrancesco, a former master student in our lab, OCR was measured before and after the addition of inhibitors, in order to derive several parameters of mitochondrial respiration for all cells in culture wells of GFP, WT NS, G392E NS and dNS lines differentiated for six days. Initially, baseline cellular OCR is measured, from which basal respiration can be derived by subtracting non-mitochondrial respiration. Next, oligomycin, a complex V inhibitor, is added and the resulting OCR is used to derive ATP-linked respiration (by subtracting the oligomycin rate from baseline cellular OCR) and proton leak respiration (by subtracting non-mitochondrial respiration from oligomycin rate). Next, carbonyl cyanide-p-trifluoromethox-yphenyl-hydrazol (FCCP), a protonophore, is added to collapse the inner membrane gradient, allowing the electron transport chain to function at its maximal rate, and maximal respiratory capacity is derived by subtracting non-mitochondrial respiration from the FCCP rate. Lastly, antimycin A, inhibitor of complex III, is added to shut down the electron transport chain function, revealing the non-mitochondrial respiration. The mitochondrial reserve capacity is calculated by subtracting basal respiration from maximal respiratory

capacity (see Methods for a graphic explanation). As reported in figure 11, none of the parameters evaluated showed variations in our cell lines.

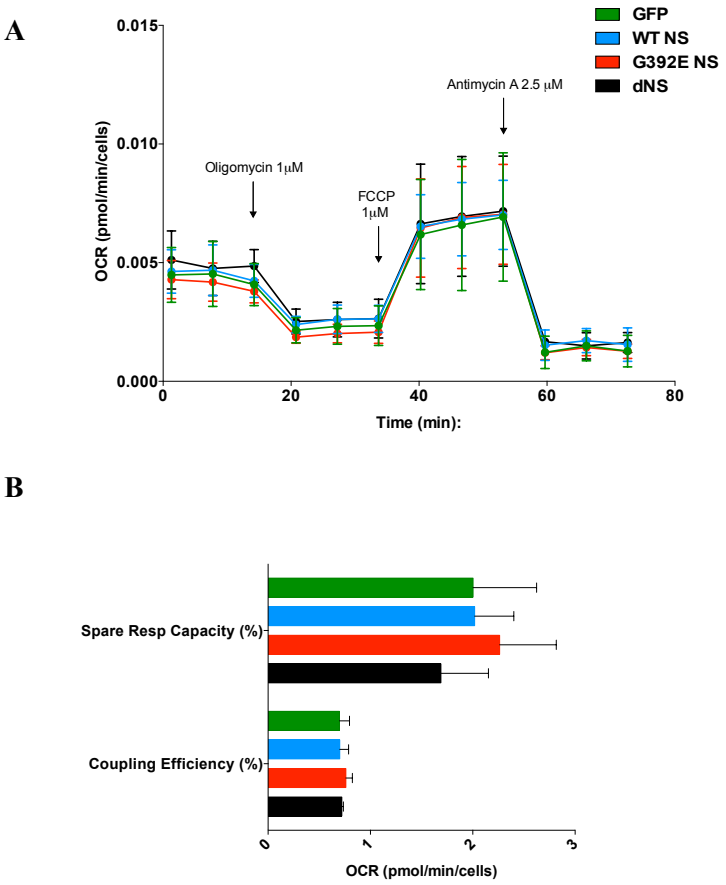

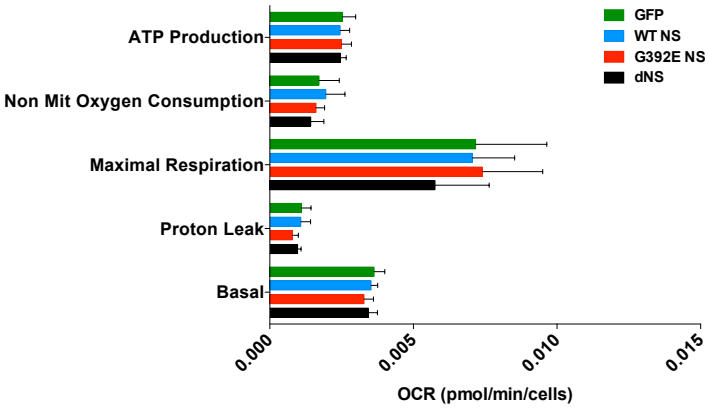

Figure 11. Seahorse analysis of differentiated NSPCs. A. NSPCs were differentiated for 6 days and Seahorse assay was performed, by recording the oxygen consumption rate of each culture well, in the presence of pharmacological treatments as described in the main text **B.** Mitochondrial metabolic parameters evaluated in all four cell lines. Data are mean ± SEM, n=5, one-way ANOVA.

G392E NS cells show a reduction in ER-mitochondria membrane contact sites

Recent studies support the importance of the communication between the ER, where mutated NS accumulates, and mitochondria. ER-mitochondria contact sites are highly dynamic structures controlling lipid and calcium homeostasis and mitochondrial metabolism, as well as several intracellular processes and signaling pathways. Since NS polymers accumulate inside the ER, we investigated the crosstalk between ER and mitochondria by assessing the extent of their contact regions, the mitochondria associated membranes (MAMs), comparing MAMs in G392E NS neurons to those of WT NS ones. In collaboration with Dr. Giovanna Galliciotti (University Medical Center Hamburg-Eppendorf, Germany), we double stained cells differentiated for six days for Tom20, an import channel of the outer mitochondrial membrane, and KDEL, the ER retention motif found in many ER resident proteins. By using stimulated emission depletion (STED) microscopy, a high-resolution confocal microscopy approach, we quantified the overlapping between these two organelles with Imaris Microscopy Software and found that G392E NS cells had a reduced contact between ER and mitochondria when compared to WT NS cells (Fig. 12). This result was also confirmed by western blot analysis of some proteins characteristic of the contact regions between ER and mitochondria which are directly involved in the transport of calcium between the two organelles, Sigma1R, VDAC and IP3R. As shown in Fig. 13 all three proteins show a significant decrease in G392E NS cells.

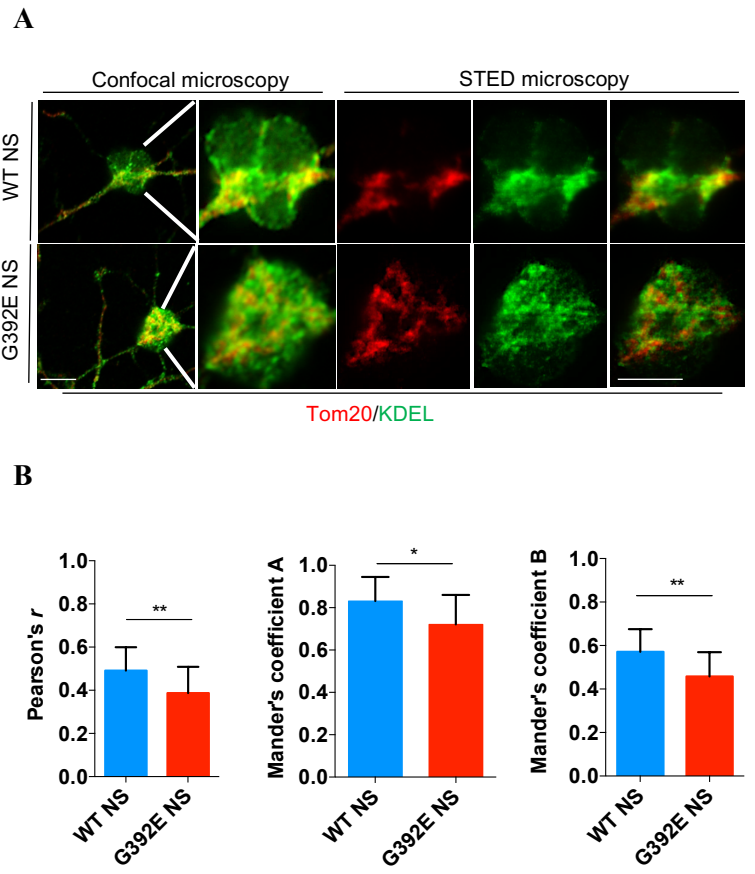

Figure 12. Evaluation of ER-mitochondria contact regions with STED confocal microscopy. NSPCs were differentiated for 6 days, double stained for Tom20 (red), and KDEL (green), and analysed with STED confocal microscopy and Imaris Microscopy Software. **A.** Immunofluorescence panels of regular confocal and STED confocal microscopy of representative cells. **B.**

Pearson's and Mander's coefficients (A= overlapping of red fluorescence on green fluorescence, B= overlapping of green fluorescence on red fluorescence) measured in cells expressing either WT or G392E NS. Data are mean ± SEM, n=3 (15-20 neurons analyzed per experiment), t-test: **p ≤ 0.01, * p ≤ 0.05. Scale bar 10μm.

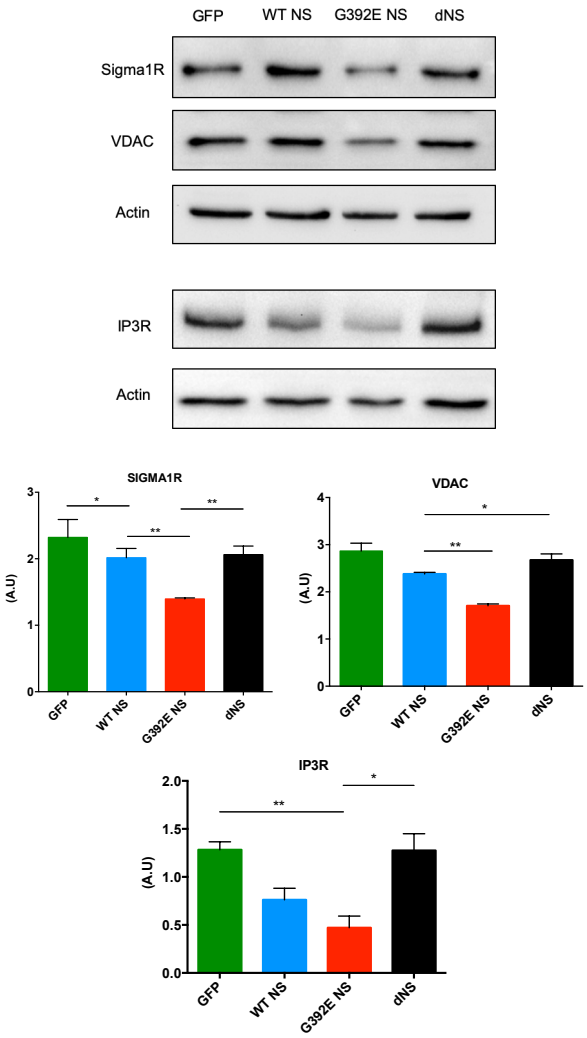

Figure 13. Evaluation of proteins characteristic of ER-mitochondria contact sites. Samples were resolved by 10% w/v acrylamide SDS PAGE and

analysed by western blot with an anti-Sigma1R, -VDAC and -IP3R antibodies. The same membrane was probed for the housekeeping enzyme beta actin as a loading control. n = 3; t-test: ***p ≤ 0.001, **p ≤ 0.01, * p ≤ 0.05.

Discussion

In this part of my PhD project, we investigated the cellular consequences of the presence of NS polymers in the ER by expressing a highly polymerogenic FENIB variant, G392E NS, in NSPCs. Previous work in the lab started from an unbiased analysis of the entire mRNA profiles of NSPCs expressing G392E NS or negative control GFP differentiated *in vitro* to produce neurons. This analysis identified 747 genes significantly altered in G392E NS cells, either up-regulated (623) or down-regulated (124). Among these, we selected 17 overexpressed and 4 under expressed genes as particularly relevant to our studies due to their role in oxidative stress, and demonstrated that the expression of G392E NS induced adaptation of NSPCs to pro-oxidant conditions, and when challenged by pharmacological inhibition of the anti-oxidant response they died by apoptosis (Guadagno et al., 2017). Because these cell lines can be amplified only for a limited number of passages (usually between 15 and 20 times), we started the present work by recreating the same NSPC lines and demonstrating that our *in vitro* differentiation protocol produced neurons and the overexpressed genes behaved as published in our previous work (Guadagno et al., 2017). The expression of *Dcx*, a marker of differentiating neuroblasts, was strongly increased in our differentiation conditions, indicating that, in agreement with previous publications (Onorati et al., 2011), our six days differentiation protocol produces immature neurons, nearly 60% of the total culture by positivity to βIII tubulin, and that our *in vitro* system can recapitulate the upregulation of endogenous NS expression observed during early stages of neurogenesis *in vivo*, reaching nearly 30% of

the levels found in mouse telencephalic tissue at E13.5. Using the newly generated cell lines expressing GFP, WT NS, G392E NS and delta NS we confirmed that in differentiating conditions WT NS was correctly secreted as a monomer into the culture medium, while G392E NS accumulated as polymers within ER and delta NS was degraded by ERAD, in accordance with the handling of NS described in other cell model systems (Miranda et al., 2004 and 2008; Krueger et al., 2009; Davis et al., 2009; Roussel et al., 2013), as well as our results in the first work published using NSPCs (Guadagno et al., 2017).

Recent research has demonstrated the role of oxidative stress in neurodegenerative diseases and the importance of the communication between the ER and mitochondria, the major organelle involved in the response to oxidative stress. Mitochondrial function is essential to neuronal processes such as energy production, Ca^{2+} regulation, maintenance of plasma membrane potential, protein folding by chaperones, axonal and dendritic transport and the release and re-uptake of neurotransmitters at synapses (Chan, 2006a, b; Hoppins et al., 2007; Zhang et al., 2007). Moreover, axonal transport of mitochondria is required for neuronal function (Hollenbeck et al., 2005). Several evidences support a role for mitochondrial morphology and dynamics in neurodegenerative disorders (Maharjan et al., 2014). Recent studies about apoptosis have uncovered a central role for mitochondria, showing the disintegration of the mitochondrial network and the formation of punctiform mitochondria located close to the nucleus early during apoptosis (Karbowski et al., 2002; Desagher et al., 2000). We thus decided to look at the mitochondrial network

in our neuronal model for the dementia FENIB, where we identified three types of mitochondrial distribution: network mitochondria, typical of healthy cells and homogeneously distributed throughout the neuronal cytoplasm; perinuclear mitochondria, in which mitochondria are found clustered close to the nucleus, generally on one side; and fragmented mitochondria, distributed all around the nucleus with a clear punctuate staining. Mitochondrial fragmentation is typical of neurodegenerative processes, while clustering of mitochondria close to the nucleus has been shown during the initial steps of caspase-independent apoptosis, as with tau overexpression in Alzheimer's disease (Ebneth et al., 1998; Satoh et al., 2005; Trinezek et al., 1999). In basal conditions, differentiated NSPCs expressing G392E NS showed a higher proportion of cells with mitochondrial clustering close to the nucleus, suggesting that NS polymers induce mitochondrial alterations as part of their toxic effect. Moreover, since the addition of culture medium containing NS polymers secreted by G392E NS cells did not cause an increase in perinuclear mitochondria in GFP cells, the increase in altered mitochondrial distribution seen for G392E NS cells should be due to the intracellular accumulation of polymers within the ER. Since alterations in mitochondrial dynamics have been described in numerous neurodegenerative disorders and under oxidative stress conditions, our results suggest that the mitochondrial phenotype observed in G392E NS cells is due to the oxidative stress induced by accumulation of NS polymers (Guadagno et al., 2017). Recent studies conducted in mouse models have shown an association between oxidative stress and the pathophysiology of the best-described serpinopathy, alpha-1 antitrypsin deficiency (A1ATD), which is caused by the

accumulation of alpha-1 antitrypsin (A1AT) polymers within the liver (Lomas et al., 2002). A1ATD mice showed higher GSTs mRNA levels but no differences were found in total GSH content if compared to control mice (Marcus et al., 2012). Furthermore, an increase in oxidative stress has been demonstrated in young patients with A1ATD before the development of severe clinical manifestations (Escribano et al., 2014). Serum measurements in these patients showed low total and reduced GSH as well as reduced catalase activity, supporting the implication of oxidative stress in A1ATD associated to the presence of A1AT polymers. We have reported recently the activation of an adaptive antioxidant response in our G392E NS cells that masked the neurotoxic effect of NS polymer accumulation, and which could be unmasked with a chelator of glutathione (DEM). We now show that the same treatment leads to the appearance of fragmented mitochondria in our NSPCs, with G392E NS neurons as the most sensitive to the pro-oxidant treatment, confirming the link between oxidative stress and mitochondrial alterations in our model of FENIB. In the opposite way, we have found that two antioxidant molecules, melatonin and α-tocopherol, can decrease the proportion of neurons with perinuclear mitochondria to levels similar to those of WT NS and GFP control neurons. Melatonin has hormonal as well as anti-inflammatory and anti-apoptotic properties (Calvo et al., 2013), is implicated in energy metabolism and thermoregulation in mammals and plays also a vital role in the lessening of neonatal hypoxia–ischemia induced ER stress in neural cells of newborn rats (Carloni et al., 2014). The experimental evidence supports its actions as a direct free radical scavenger (Hardeland et al., 1995; Allegra et

al., 2003), as an indirect antioxidant by stimulating antioxidant enzymes (Reiter et al., 2000), by stimulation of the synthesis of glutathione (Urata et al., 1999), by protection of antioxidative enzymes from oxidative damage (Mayo et al., 2003), and due to its ability to increase the efficiency of mitochondrial electron transport chain thereby lowering electron leakage and reducing free radical generation (Okatani et al., 2003). Similarly, α-tocopherol, or vitamin E, is a lipid soluble antioxidant that protects cell membranes from oxidative damage and has a protective action at nanomolar and micromolar concentrations against H_2O_2-induced brain cortical neuron death (Zakharova et al., 2017). We tested both antioxidants after performing dose-response curves and found a significant rescue of the perinuclear mitochondrial phenotype for G392E NS cells. These results confirm the link between oxidative stress and mitochondrial alteration in these cells and suggest that overexpression of cellular antioxidant defenses together with exogenous administration of antioxidant molecules promotes a reversion of the altered mitochondrial distribution, reverting it to control levels.

Our results show that cells with altered mitochondrial distribution generally lack well-developed neurites, as seen by co-staining of mitochondria and polymerised actin. In agreement with this observation, we found that G392E NS cells, compared with the WT ones, had shorter neurites. Recent evidences indicate that there is a constant crosstalk between the actin cytoskeleton and the release of ROS by mitochondria (induced by either hypo- or hyper-polarization of the mitochondrial membrane) (Wilson and Gonzalez-Billault, 2015). Intracellular ROS production is needed for proper cell

migration and chemotaxis, which are actin-dependent processes especially for neurons (Roberts et al., 1999; Ambruso et al., 2000; Kim and Dinauer, 2001). Whereas physiological ROS production is needed for proper cytoskeleton polymerisation, oxidation tends to disrupt polymerisation and impair cytoskeletal dynamics under oxidative stress conditions (Munnamalai and Suter, 2009; Hung et al., 2018; Morinaka et al., 2011; Wilson et al., 2015). Indeed, there are evidences on the role of ROS as promoters of neuritic growth influencing the state of actin polymerisation under physiological conditions (Munnamalai and Suter, 2009), but it has also been demonstrated that the persistent presence of ROS causes carbonylation of actin, producing the loss of lamellipodia and the arrest of cellular plasticity (Barth et al., 2009). Our findings suggest the possibility that the chronic oxidative condition promoted by G392E NS expression influences the cytoskeletal dynamics of neurons, during dendrite formation or during the definition of synaptic spines, but further investigations are needed to understand link between oxidative stress, altered mitochondrial distribution and cytoskeleton dynamics in our cellular model of FENIB.

To better understand the extent of the mitochondrial perturbation in our G392E neurons we looked at one of the most important parameters of mitochondria, its inner membrane potential (ψ_m), a sensitive indicator of the energy state of mitochondria and cell viability. Our results support a decrease in ψ_m of G392E NS cells differentiated to neurons, compared to cells overexpressing WT NS. The loss of membrane potential can have different meanings and there are conflicting data in the literature regarding the connection

between membrane potential and ROS genesis (Duchen et al., 2004). Depolarization of mitochondria following excessive ROS production is an early sign of mitochondrial dysfunction and precedes many other signs of cell injury (Zamzami et al. 1997). In several cellular models a concomitance between the loss of inner mitochondrial membrane potential and an increase in ROS genesis has been highlighted, with a consequent increase in oxidative stress (Satoh et al. 1997; Wood-Kaczmar et al 2008; Gottlieb et al. 2000; Ricci et al. 2003). Furthermore, oxidative damage affects mitochondria at different levels, resulting in increased mtDNA mutations and protein and lipid oxidation. Recent studies suggest a central role for mitochondrial potential and oxidative damage to the organelle in the gradual decline of brain functions during aging (Nicholls et al., 2004). In agreement with this, Xiong et al. (2002) found a 5 mV decrease in $\Delta\psi$ of acutely isolated cerebellar slices from old mice compared to young ones. In collaboration with the laboratory of Prof. M. Duchen at UCL (London, UK), we analysed our NSPCs by Seahorse assay, a well-stablished approach to measure key mitochondrial bioenergetic and metabolic parameters in whole cell populations of cultured wells. We found no significant differences between the four cell lines, probably due to the mixed character of our differentiated cultures, which contain glial as well as neuronal cells, but also suggesting that mitochondrial function is not excessively altered in G392E NS neurons, in agreement with the lack of neuronal death observed for these cells in basal conditions.

The ER and mitochondria are intimately related, with the homeostasis of both organelles finely tuned by their

interaction at particular regions of contact between their membranes, the mitochondria-ER sites (MAMs). Since NS polymers accumulate inside the ER, we have also investigated the crosstalk between ER and mitochondria by assessing the extent of MAMs in G392E NS neurons compared to WT NS ones. Our results show a decrease in the area of contact between the two organelles and a concomitant decrease of proteins characteristics of these sites. These results directly link the alterations due to the expression of the polymerogenic G392E NS with the mitochondrial alterations described above. The contacts between ER and mitochondria are abundant in all neuronal compartments and often the ER forms a network that "embraces" the mitochondria (Wu et al., 2017). The molecular composition of MAMs is very heterogeneous in different eukaryotic cells and, in mammals, includes an abundant and complex range of proteins (Lee e Min, 2018). Mitochondrial proximity to the ER governs especially the dynamics of calcium transfer from the ER to mitochondria (Mironov et al., 2005), relying particularly in the initial complex formed by interaction between IP3R (inositol triphosphate receptor, localized in the ER membrane), Grp75 (glucose-regulated protein 75) VDAC (voltage-dependent anion channel 1, localized at the outer mitochondrial membrane) and Sigma-1 receptor (localized in the ER membrane). The impairment of RE-mitochondria communication has a decisive role in metabolic and neurodegenerative diseases and in cancer. There are numerous studies in which structural and functional changes have been observed at MAMs in neurodegenerative diseases such as Alzheimer’s and Parkinson’s diseases (Lee and Min, 2018). Although the role of MAMs in neurodegeneration has not yet been clarified, data on

Alzheimer's disease suggest that increased communication between ER and mitochondria may enhance neuronal death, probably due to an increase in Ca^{2+} influx within the mitochondria (Hedskog et al. 2013). On the contrary, in Parkinson's disease neurodegeneration seems related to disintegration of MAMs: α-synuclein has been identified at the level of these sites (Guardia-Laguarta et al., 2014), and mutations that affect this protein in patients with familial Parkinson's disease promote a decrease in ER-mitochondria contact sites, as well as greater fragmentation of the mitochondrial network (Cali et al., 2012), reminiscent of our own findings for FENIB.

In summary, our present work shows for the first time the interconnection between NS polymer deposition and oxidative stress with ER-mitochondria communication and mitochondrial alterations in FENIB. Our data support that expression of polymerogenic mutant NS causes pro-oxidative conditions in neuronal cells that alter the dynamics and functionality of mitochondria. These new aspects of the neurodegenerative dementia FENIB are consistent with recent findings showing that oxidative stress and mitochondrial dysfunction lead to neurodegeneration and aging and underlie the pathology of several neurodegenerative disorders.

Methods

Creation of transgenic lines of neural stem progenitor cells with stable expression of neuroserpin

In previous work, the open reading frame (ORF) of human neuroserpin (NS) was amplified by PCR and subcloned into the pTP6 expression vector. This vector contained the CAGG promoter followed by the NS gene, an internal ribosome entry site (IRES) and the gene for puromycin resistance, allowing selection for simultaneous expression of both genes. Here, early passage neural stem progenitor cells (NSPCs) obtained as described in the next section were transfected with pTP6-NS in three different versions: WT NS, G392E NS and delta NS, a truncated version of NS lacking the last 134 aminoacids and used as a misfolding protein control (Davis et al., 2009). NSPCs were transfected with Amaxa Nucleofector and Neural Stem Cell Nucleofector kit (Lonza) according to manufacturer instructions. Two days after transfection, NSPCs with stable integration of the pTP6-NS transgene were selected and expanded by adding puromycin (1-1,6 μg/ml) to the culture medium. A control NSPC line expressing pTP6-GFP was already available and has been used here as a negative control. The plasmids used confer resistance to puromycin to cells that integrate the plasmid itself. This resistance allows us to select and maintain cells by constant culture in the presence of puromycin 1 μg/ml.

Cell cultures

NPCs were obtained from embryonic cortex of E13.5 mice, sacrificed by cervical dislocation. The tissues were incubated in Dulbecco's modified Eagle's Medium (DMEM) for 20 min at 37°C and then mechanically dissociated. The cells obtained were transferred into pretreated T25 plastic flasks with 10 mg/ml of poly-ornithine (Sigma) and 5 µg/ml of laminin (Sigma) in basal medium consisting of DMEM/F12, 1% penicillin/streptomycin (Sigma), 0.1 M L-glutamine (Sigma), 23.8 mg/100ml Hepes (Sigma), 7.5% $NaHCO_3$, 0.6% glucose (Sigma). Basal medium was completed with 20 ng/ml of human epidermal growth factor (hEGF, R&D), 10 ng/ml of basic fibroblast growth factor (bFGF, R&D), 1% B-27 supplement (Gibco Life Sciences) and 1% N2 supplement (Gibco Life Sciences) to get complete medium. Once the confluence was reached, the cells were dissociated with Accutase (Sigma) and again seeded on flasks. The cells were kept at 37°C in a 5% CO_2 atmosphere.

Differentiating conditions

For neuronal differentiation NSPCs were plated in expansion medium (20,000 cells/cm2) and 24 h later this was replaced with basal medium containing 10 ng/ml bFGF, 1% N2, 1% B27, 0.5 µM DAPT (Tocris Bioscience) and 40 ng/ml hBDNF (Peprotech), termed neuronal differentiation medium. Three days later this medium was replaced with fresh medium. After 6 days under these conditions, NSPCs differentiate into a mixed culture of neurons (around 50-60%) and glia or not

completely differentiated cells (as reported in Soldati et al., 2012).

Protein analysis

Cell lysates from proliferative or differentiated cells were obtained by adding 80 µl of complete lysis buffer (150 mM NaCl, 50 mM TRIS-Cl, pH 7.5) plus 1% (v/v) Nonidet P-40 and 1X protease cocktail inhibitor (Sigma Aldrich) directly into the flask (T25), using a cell scraper (Corning) for cell detachment and lysis, followed by recovering of the lysis volume and incubation on ice for 20 min. The lysate was cleared by spinning at top speed (17,000 g) in a bench centrifuge at 4°C for 15 min. Total protein concentration of proliferative cell lysates was measured by Bradford assay (Bio-Rad), using bovine serum albumin (BSA, stock 1 mg/ml) for the standard curve. Two µl of sample or each standard point were diluted in 63 µl of distilled water, and 2 µl of lysis buffer were added to each standard point to correct for the background signal due to the presence of Nonidet P-40. Forty µl of Bradford reagent were added to each sample, mixed by pipetting and incubated for 5 min in the dark at room temperature. The absorbance was measured in a plate reader (Glomax-Multi Detection System, Promega) at 595 nm. For culture medium supernatant analysis, the sample was centrifuged at 100 g for 5 min to remove dead cells and cell debris.

RNA extraction and RT-PCR

NSPCs plated in T25 flasks were lysed in 400 µl/flask of RLT buffer and total RNA was extracted by following the kit's instructions (RNeasy Mini Kit QIAGEN). For proliferative cells, 50 µl of RNase-free water were used for RNA elution. To increase the recovery of total RNA from differentiated cells, a carrier RNA was added to the RLT buffer, and 20 µl of RNase-free water were used for RNA elution. RNA was quantified by using the Thermo Scientific NanoDrop 2000 spectrophotometer. RNA sample template was used for retro-transcription with Thermo Scientific RevertAid First Strand cDNA synthesis kit (Thermo Scientific). Five hundred µg of RNA sample template were added into a sterile, nuclease-free tube on ice, 2 µl of oligo (dT) primer was added and solution brought to volume (12 µl) with nuclease-free water. Subsequently, the following reagents were added in the indicated order: 4 µl of 5X reagent buffer; 1 µl of RiboLock RNase inhibitor (20 u/µl); 2 µl of 10 mM dNTP mix; 1 µl of RevertAid M-MuLV reverse Transcriptase (200 u/µl). Samples were gently mixed, centrifuged and incubated for 60 min at 42 °C. Reaction was terminated by heating at 70 °C for 15 min.

Real-time polymerase chain reaction

For real-time polymerase chain reaction (PCR), RNA was reverse-transcribed using the Qiagen QuantiTect reverse transcription kit and amplified on a Rotor-Gene Q (Qiagen), using Qiagen SYBR Green PCR kits. Primers for RT-PCR and real-time PCR were purchased from Sigma-Aldrich. Relative

gene expression levels in different samples were determined with the built-in comparative quantitation method using *EF1α* or *Rpl19* as a normalizer.

Denaturing gel electrophoresis and western blot analysis

Adequate volumes of cell lysates from proliferative cells to obtain equal loading of total protein were mixed with 4X loading buffer containing Tris-HCl 125mM pH 6.8, 2% sodium dodecyl sulfate (SDS), 10% glycerol, 0.02% bromo-phenol blue, 5% β-mercaptoethanol and incubated at 95°C for 10 min. Since very low protein quantities were extracted from differentiated cells, the maximum volume (40 µl) of cell lysates and culture media were loaded in each lane, using the same loading buffer. Samples were then analysed in 1 mm, 10% (w/v) polyacrilamide gel electrophoresis gels (PAGE) (Table 1), with SDS running buffer (Tris 25 mM, glycine 250 mM and SDS 3 mM) at 90 V. After SDS-PAGE, proteins were transferred from the gels into Immobilion P membrane, PVDF (Millipore Corp., Milano, Italy) at 200 mA for 2 h for western blot analysis, using. transfer buffer (Tris 20 mM, glycine 140 mM) with 5% (v/v) methanol. After transfer, the membrane was washed in PBT [PBS plus 0.1% (v/v) Tween 20] and blocked for 2 h in PBT plus 5% (w/v) dried skimmed milk powder (Marvel Dried Milk). The membrane was incubated with polyclonal anti-NS antibody (whole serum) diluted 1:10,000 in blocking buffer (PBS, BSA 3% plus sodium azide 0.1%) or with antigen-purified rabbit polyclonal anti-NS antibody (1 µg/ml), both a kind gift of Prof. David Lomas (UCL, London, UK) in the same blocking buffer overnight at 4°C. The following day, the membrane was washed three

times for 5 min in PBT, and then incubated with anti-rabbit IgG-horseradish peroxidase secondary antibody diluted at 1:50.000 in PBT-milk for 90 min. The membrane was washed six times for 5 min with PBT and three times for 5 min with PBS before developing with ECL substrate (LiteAblot Plus Enhanced Chemiluminescent Substrate, Euroclone EMP 01005 or LiteAblot Turbo Extra-sensitive Chemiluminescent Substrate, Euroclone EMP012001). Chemiluminescence was revealed by autoradiography or in a ChemiDoc instrument (BioRad). Rabbit polyclonal anti-actin (Abcam) was used as a loading control.

Non-denaturating gel electrophoresis and western blot analysis

Samples from differentiated cells were mixed with loading buffer containing Tris-HCl 125 mM pH 6.8, 10% glycerol, 0.02% bromo-phenol blue, and analysed in 1 mm, 7.5% non-denaturating PAGE gel (Table 1) by electrophoresis using two different running buffers (anode - external chamber: Tris 100mM pH 7.8, adjusted with 5 M HCl, and cathode - internal chamber: Tris 53mM and glycine 68mM, pH 8.9), at 90 V. Proteins were transferred from the gels onto Immobilion P membrane, PVDF (Millipore) at 200 mA for 2 h in transfer buffer (Tris 20 mM, glycine 140 mM) for western blot analysis following the same protocol described above.

SDS - PAGE

	10% RESOLVING (ml)	5% STACKING (ml)	
H_2O	1,9	0,68	H_2O
30% acrylammide	1,7	0,17	30% acrylammide
1,5M TRIS (ph 8.8)	1,3	0,13	1 M TRIS (ph 6.8)
10% SDS	0,05	0,01	10% SDS
10%APS	0,05	0,01	10%APS
TEMED	0,02	0,001	TEMED
Total volume	5	1	Total volume

NON DENATURING - PAGE

	7,5% RESOLVING (ml)	5% STACKING (ml)	
H_2O	2,5	1,37	H_2O
30% acrylammide	1,25	0,343	30% acrylammide
1,5M TRIS (ph 8.8)	1,25	0,215	1 M TRIS (ph 6.8)
10%APS	0,018	0,021	10%APS
TEMED	0,004	0,003	TEMED
Total volume	5	1	Total volume

Table 1. SDS and non-denaturing gel preparation. Volumes refer to gels that are 1 mm in thickness.

Fluorescence staining for mitochondrial distribution

Cells for fluorescence staining were grown on coverslips pre-treated with poly-ornithine and laminin, in 24-well plates. Mitochondria were stained with Mitotracker Red CMX Ros ® (Mitotracker) (Life Technologies) at a final concentration of 100 nM in culture medium for 10 min at 37°C. Next, cells were rapidly washed in pre-warmed PBS and immediately fixed in 4% (v/v) paraformaldehyde (PFA) for 15 min. Cells were then incubated with permeabilization solution (0,1% triton in PBS) for 10 min, washed and incubated with 6-diamidino-2 phenylindole (DAPI) for 10 minutes. Cells were then mounted in Fluorosave (Calbiochem, through CN Biosciences, Nottingham, UK) containing 2% (w/v) 1,4-diazabicyclo [2.2.2] octane (DABCO) and analysed by fluorescence microscopy with an Apotome fluorescence imaging system (Zeiss) at 63x magnification. At least one hundred fifty cells were evaluated for each condition, and the mitochondrial distribution was classified into three categories as described in the Results section. As a positive control, NSPCs cells expressing GFP were incubated with 100 μM of H_2O_2 for 10 minutes. After the incubation time, cell medium was replaced with fresh differentiation medium and cultured for 24 h at 37°C. After 24 h, cells were stained with Mitotracker as described above.

Neurotoxicity and antioxidant experiments

Hydrogen peroxide (H_2O_2)

NSPCs were cultured in differentiation medium for 6 days in a 24-well plate. At day 5, cells were treated with 100 μM H_2O_2 for 30 min. After the incubation period, cell medium was replaced with fresh medium and cultured for 24 h at 37°C before fixation in 4% (v/v) PFA for 15 min.

Diethyl maleate (DEM)

NSPCs cells were cultured in differentiation medium for 6 days in a 24-well plate. At day 5 of differentiation, cells were pre-incubated in presence or absence of 50 μM diethyl maleate (DEM, Sigma Aldrich) at 37°C for 1 h. After the incubation period, cell medium was replaced with fresh differentiation medium and cultured for 24 h at 37°C. After this, cells were stained with Mitotracker for evaluating the mitochondrial distribution, washed once in PBS and fixed in 4% (v/v) PFA for 10 minutes.

α-Tocopherol and melatonin

NSPCs cells were cultured in differentiation medium for 6 days in a 24-well plate. At day 4 of differentiation, cells were incubated in the presence or absence of 10 μM tocopherol or melatonin (Sigma Aldrich) for the last 48 h of differentiation. After 48 h cells were stained with Mitotracker for evaluating the mitochondrial distribution, were washed once in PBS and fixed in 4% (v/v) PFA for 10 minutes.

Fluorescence staining for cellular morphology

Cells were grown as indicated above. After 6 days of differentiation cells were rapidly washed in pre-warmed PBS and immediately fixed in 3.7% (v/v) paraformaldehyde for 15 min. After 3 washes with PBS, cells where stained with phalloidin conjugated with Alexa Fluor 488 (Thermo Fisher Scientific) at the final concentration of 50 µg/ml for 40 min. Cells were then washed and incubated with permeabilization solution (0,1% Triton in PBS) for 10 min, then washed again and incubated with DAPI for 10 min and mounted in Fluorosave plus 2% (w/v) DABCO and analyzed with an Apotome fluorescence imaging system (Zeiss) at 63x magnification.

Sandwich ELISA

Unless stated otherwise, all steps were carried out at room temperature and using 50 µl/well. 96-well plates (Corning) were used for NS detection by using a monoclonal antibody specific for NS polymers (7C6, Miranda et al., 2008). Plates were coated overnight at 4°C with antigen-purified rabbit polyclonal anti-NS antibody at 4 µg/µl for plate in PBS. Next, wells were washed 3 times with 0.9% w/v NaCl, 0.05% v/v Tween 20 and blocked for 2 h with 300 µl/well of blocking buffer (PBS, 0.25% w/v BSA, 0.05% v/v Tween 20, 0.01 w/v sodium azide). Standards (recombinant purified WT or polymerised mutant NS) and unknown samples (culture medium supernatants) were incubated overnight at 4°C. Standard curves were prepared by making serial dilutions of standards with known concentration. The following day, the

wells were washed as described above and incubated with the monoclonal 7C6 antibody (1 μg/ml) diluted in blocking buffer for 2 h. Bound monoclonal antibodies were detected with rabbit anti-mouse HRP antibody (1:20,000 in blocking buffer without sodium azide) for 1 h. After developing for 10 min with TMB substrate solution and stopping the reaction with 1M H_2SO_4, HRP activity was measured in a Glomax plate reader at 450 nm. For the analysis, WT NS and polymerised NS standard curves were used to calculate the concentration of WT and mutant NS in the cell lysates and culture media, respectively.

Evaluation of the inner mitochondrial membrane potential with the JC-1 cationic dye

Cells were grown on coverslips as above. After 6 days of differentiation cells were stained with the JC-1 Mitochondrial Membrane Potential Detection Assay Kit (Biotum), at a 1:100 dilution for 15 min. After a wash in PBS, cells were mounted on coverslips adding a small drop of PBS to facilitate the adhesion and living cells were analyzed by confocal microscopy (Zeiss) with 63x magnification. JC-1 aggregates (red fluorescence) and monomers (green fluorescence) were imaged simultaneously with a dual band-pass filter for fluorescein (Ex/Em 490/520 nm) and rhodamine (Ex/Em 540/570 nm). The confocal images were analyzed and quantitated as the ratio of aggregate/monomer using image analysis software “Image J” (NIH software), a public domain Java image processing program. Confocal images are pseudo red-green-blue (RGB) color images that were converted to 8 bit-gray scale images and splitted into images that showed

only red or green fluorescence. At least one hundred images for each sample were evaluated.

Seahorse assay

Oxygen consumption rates (OCR) were measured with the Seahorse XFe96 Analyser (Agilent) using the Seahorse XFe96 FluxPak (Agilent, 102416-100). NSPCs were grown (day 0, plating at 8,000 cells/well) and differentiated on pre-coated Seahorse XF96 cell culture microplates for 6 days. The XFe sensor cartridge was hydrated overnight using the Seahorse XF Calibrant Solution at 37°C in a 0% CO_2 incubator the day before the experiment. On the day of the assay, the cells were washed twice and then incubated with 175 µL of recording medium, prepared using Seahorse XF base medium (Agilent, 102353-100), 1 g/L glucose (Sigma), 1 mM sodium pyruvate (Sigma) and 2 mM glutamate (Sigma), for 1 h in a 0% CO_2 incubator. In the meantime, the hydrated XFe sensor cartridge was loaded with 25 µL of 1 µM olygomicin (Sigma) in port A, 25 µl of 1 µM of carbonyl cyanide-p-trifluoro methoxyphenyl hydrazone (FCCP) (Sigma) in port B and port C, and 25 µl of 2,5 µM antimycin A (Sigma) in port D. The loaded cartridge and the utility plate were placed in the Seahorse XFe96 Analyzer for calibration and, after the replacement of the utility plate with the one containing the cells, The Seahorse XF Mito Stress assay was performed following this protocol: 1) equilibrate: 18 min; 2) OCR reading: 3 cycles of 3 minutes Mix, 0 minutes Wait and 3 minutes Measure; 3) port A injection; 4) OCR reading as 2; 5) port B injection 6) OCR reading as 2); 7) port C injection; 8) OCR reading as 2; 9) port

D injection; 10) OCR reading as 2. All the parameters evaluated are graphically explained in the figure below.

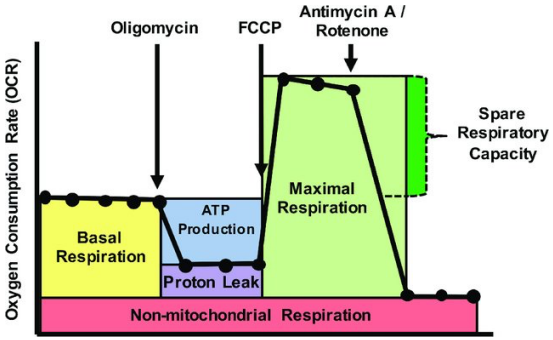

After the assay the cells were stained with 2.5 µM Hoechst (Thermo-Fisher Scientific) for 10 min and counted using the ImageXpress Micro XLS Widefield High-Content Analysis System.

Immunocytochemistry for evaluation of ER-mitochondria contact points

Cells for immunocytochemical staining were grown as described above for fluorescence staining. After 6 days of differentiation, cells were rapidly washed in pre-warmed PBS and immediately fixed in 3.7% (v/v) PFA for 15 min and washed again. Cells were then incubated with permeabilization solution (0.1% Triton in PBS) for 10 min, then incubated for 1 h with blocking solution (0.1% Triton, 0.5% BSA, 2% normal goat serum, 5 mM glycine, 0.1% sodium azide in PBS) and incubated in primary antibody anti-rabbit Tom20 (Santa Cruz Biotechnologies) and anti-mouse

KDEL (Enzo Life Science) overnight at 4°C. The cells were then washed and incubated with both secondary antibodies (anti-rabbit-Alexa 594 and anti-mouse-STAR 635P) for 60 min in blocking solution, washed and mounted in Fluorosave containing 2% (w/v) DABCO. Imaris Microscopy Software was used for the quantification of the merge regions, calculating Pearson's coefficient and both Mander's coefficients (red over green and green over red). At least 15-20 neurons from each sample were evaluated, for a total of 45-60 cells.

Statistical analysis

All experiments were performed at least three times as independent biological samples. The results of all experiments were expressed as mean ± standard error of the mean (M ± SEM). Statistical analysis of the data was conducted using the t-student test or ANOVA by using Prism5 (Graph-Pad 5 Software Inc.) or Microsoft Excel. Differences were considered significant with a value of $p \leq 0.05$ (*), $p \leq 0.01$ (**), or $p \leq 0.001$ (***).

References

Allegra, M., Reiter, R.J., Tan, D.-X., Gentile, C., Tesoriere, L., and Livrea, M.A. (2003). The chemistry of melatonin's interaction with reactive species. J. Pineal Res. *34*, 1–10.

Ambruso, D. R., Knall, C., Abell, A. N., Panepinto, J., Kurkchubasche, A., Thurman, G., et al. (2000). Human neutrophil immunodeficiency syndrome is associated with an inhibitory Rac2 mutation. *Proc. Natl. Acad. Sci. U S A* 97, 4654–4659. doi: 10.1073/pnas.080074897.

Barth, Brian M., Shelli Stewart-Smeets, e Thomas B. Kuhn. Proinflammatory Cytokines Provoke Oxidative Damage to Actin in Neuronal Cells Mediated by Rac1 and NADPH Oxidase. Molecular and Cellular Neurosciences 41, n. 2 (2009): 274–85. https://doi.org/10.1016/j.mcn.2009.03.007.

Calì, Tito, Denis Ottolini, Alessandro Negro, e Marisa Brini. α-Synuclein Controls Mitochondrial Calcium Homeostasis by Enhancing Endoplasmic Reticulum-Mitochondria Interactions. The Journal of Biological Chemistry 287, n. 22 (2012): 17914–29. https://doi.org/10.1074/jbc.M111.302794.

Calvo, J.R., González-Yanes, C., and Maldonado, M.D. (2013). The role of melatonin in the cells of the innate immunity: a review. J. Pineal Res. *55*, 103–120.

Carloni, S., Albertini, M.C., Galluzzi, L., Buonocore, G., Proietti, F., and Balduini, W. (2014). Melatonin reduces endoplasmic reticulum stress and preserves sirtuin 1

expression in neuronal cells of newborn rats after hypoxia-ischemia. J. Pineal Res. *57*, 192–199.

Carrell RW, and Lomas DA, (1997), Conformational disease, *Lancet*, 350: 134–138

Chan, DC, (2006a), Mitochondria: dynamic organelles in disease, aging, and development, *Cell*, 125: 1241-1252.

Chan, DC, (2006b). Mitochondrial fusion and fission in mammals*, Annu Rev Cell Dev Biol,* 22: 79–99.

Davis, R.L., Shrimpton, A.E., Holohan, P.D., Bradshaw, C., Feiglin, D., Collins, G.H., Sonderegger, P., Kinter, J., Becker, L.M., Lacbawan, F., et al. (1999a). Familial dementia caused by polymerisation of mutant neuroserpin. Nature *401*, 376–379.

Davis, R.L., Holohan, P.D., Shrimpton, A.E., Tatum, A.H., Daucher, J., Collins, G.H., Todd, R., Bradshaw, C., Kent, P., Feiglin, D., et al. (1999b). Familial encephalopathy with neuroserpin inclusion bodies. Am. J. Pathol. *155*, 1901–1913.

Dawwas MF, Davies SE, Griffiths WJ, Lomas DA, Alexander GJ. Prevalence and risk factors for liver involvement in individuals with PiZZ-related lung disease. Am J Respir Crit Care Med 2013;187: 502–508.

Desagher, S., and Martinou, J.C. (2000). Mitochondria as the central control point of apoptosis. Trends Cell Biol. *10*, 369–377.

Duchen, Michael R. Mitochondria in Health and Disease: Perspectives on a New Mitochondrial Biology. Molecular Aspects of Medicine 25, n. 4 (2004): 365–451. https://doi.org/10.1016/j.mam.2004.03.001.

Ebneth, A., Godemann, R., Stamer, K., Illenberger, S., Trinczek, B., Mandelkow, E.-M., and Mandelkow, E. (1998). Overexpression of Tau Protein Inhibits Kinesin-dependent Trafficking of Vesicles, Mitochondria, and Endoplasmic Reticulum: Implications for Alzheimer's Disease. The Journal of Cell Biology *143*, 777–794.

Ekeowa UI, Freeke J, Miranda E, Gooptu B, Bush MF, et al. (2010) Defining themechanism of polymerisation in the serpinopathies, *Proc Natl Acad Sci*, 107: 17146–17151.

Eriksson S, Carlson J, Velez R. Risk of cirrhosis and primary liver cancer in alpha1-antitrypsin deficiency. N Engl J Med 1986; 314:736–739.

Escribano, A., Amor, M., Pastor, S., Castillo, S., Sanz, F., Codoñer-Franch, P., and Dasí, F. (2015). Decreased glutathione and low catalase activity contribute to oxidative stress in children with α-1 antitrypsin deficiency: Table 1. Thorax *70*, 82–83.

Galliciotti, G., Glatzel, M., Kinter, J., Kozlov, S.V., Cinelli, P., Rülicke, T., and Sonderegger, P. (2007). Accumulation of mutant neuroserpin precedes development of clinical symptoms in familial encephalopathy with neuroserpin inclusion bodies. Am. J. Pathol. *170*, 1305–1313.

Gettins, Peter G. W. «Serpin Structure, Mechanism, and Function». Chemical Reviews 102, n. 12 (2002): 4751–4804.

Gooptu, B., and Lomas, D.A. (2008). Polymers and inflammation: disease mechanisms of the serpinopathies. J. Exp. Med. *205*, 1529–1534.

Gooptu, B., and Lomas, D.A. (2009). Conformational pathology of the serpins: themes, variations, and therapeutic strategies. Annu. Rev. Biochem. *78*, 147–176.

Gottlieb, E., M. G. Vander Heiden, e C. B. Thompson. «Bcl-x(L) Prevents the Initial Decrease in Mitochondrial Membrane Potential and Subsequent Reactive Oxygen Species Production during Tumor Necrosis Factor Alpha-Induced Apoptosis». Molecular and Cellular Biology 20, n. 15 (2000): 5680–89.

Guadagno, N.A., Moriconi, C., Licursi, V., D'Acunto, E., Nisi, P.S., Carucci, N., De Jaco, A., Cacci, E., Negri, R., Lupo, G., et al. (2017). Neuroserpin polymers cause oxidative stress in a neuronal model of the dementia FENIB. Neurobiol. Dis. *103*, 32–44.

Guardia-Laguarta, Cristina, Estela Area-Gomez, Cornelia Rüb, Yuhui Liu, Jordi Magrané, Dorothea Becker, Wolfgang Voos, Eric A. Schon, e Serge Przedborski. «α-Synuclein Is Localized to Mitochondria- Associated ER Membranes». The Journal of Neuroscience: The Official Journal of the Society for Neuroscience 34, n. 1 (2014): 249–59. https://doi.org/10.1523/JNEUROSCI.2507-13.2014.

Hagen TM, Yowe DL, Bartholomew JC, Wehr CM, Do KL, Park JY, Ames BN (1997) Mitochondrial decay in hepatocytes from old rats: membrane potential declines, heterogeneity and oxidants increase. *Proc. Natl Acad. Sci. USA* **94**, 3064–3069.

Hardeland, R., Balzer, I., Poeggeler, B., Fuhrberg, B., Uría, H., Behrmann, G., Wolf, R., Meyer, T.J., and Reiter, R.J. (1995). On the primary functions of melatonin in evolution: mediation of photoperiodic signals in a unicell, photooxidation, and scavenging of free radicals. J. Pineal Res. *18*, 104–111.

Hedskog, Louise, Catarina Moreira Pinho, Riccardo Filadi, Annica Rönnbäck, Laura Hertwig, Birgitta Wiehager, Pia Larssen, et al. Modulation of the Endoplasmic Reticulum-Mitochondria Interface in Alzheimer's Disease and Related Models. Proceedings of the National Academy of Sciences of the United States of America 110, n. 19 (2013): 7916–21. https://doi.org/10.1073/pnas.1300677110.

Hollenbeck PJ and Saxton WM, (2005), The axonal transport of mitochondria, *J Cell Sci*, 118: 5411-5419.

Hoppins, S., Lackner, L., and Nunnari, J. (2007). The Machines that Divide and Fuse Mitochondria. Annual Review of Biochemistry *76*, 751–780.

Hung, Clara Hiu-Ling, Sally Shuk-Yee Cheng, Yuen-Ting Cheung, Suthicha Wuwongse, Natalie Qishan Zhang, Yuen-Shan Ho, Simon Ming-Yuen Lee, e Raymond Chuen-Chung Chang. «A Reciprocal Relationship between Reactive Oxygen

Species and Mitochondrial Dynamics in Neurodegeneration». Redox Biology 14 (2018): 7–19.

Huntington, J. A. «Serpin Structure, Function and Dysfunction». Journal of Thrombosis and Haemostasis: JTH 9 Suppl 1 (2011): 26–34. https://doi.org/10.1111/j.1538-7836.2011.04360.x.

Huntington, J. A., R. J. Read, e R. W. Carrell. «Structure of a Serpin-Protease Complex Shows Inhibition by Deformation». Nature 407, n. 6806 (2000): 923–26.

Irving, J.A., Pike, R.N., Lesk, A.M., and Whisstock, J.C. (2000). Phylogeny of the serpin superfamily: implications of patterns of amino acid conservation for structure and function. Genome Res. *10*, 1845–1864.

Karbowski, M., Lee, Y.-J., Gaume, B., Jeong, S.-Y., Frank, S., Nechushtan, A., Santel, A., Fuller, M., Smith, C.L., and Youle, R.J. (2002). Spatial and temporal association of Bax with mitochondrial fission sites, Drp1, and Mfn2 during apoptosis. The Journal of Cell Biology *159*, 931–938.

Kim, C., and Dinauer, M. C. (2001). Rac2 is an essential regulator of neutrophil nicotinamide adenine dinucleotide phosphate oxidase activation in response to specific signaling pathways. *J. Immunol.* 166, 1223–1232. doi: 10.4049/jimmunol.166.2.1223.

Knott, A.B., Perkins, G., Schwarzenbacher, R., and Bossy-Wetzel, E. (2008). Mitochondrial fragmentation in neurodegeneration. Nat. Rev. Neurosci. *9*, 505–518.

Kokoszka JE, Coskun P, Esposito LA, Wallace DC (2001) Increased mitochondrial oxidative stress in the Sod2 (+/−) mouse results in the age-related decline of mitochondrial function culminating in increased apoptosis. *Proc. Natl Acad. Sci. USA* 98, 2278–2283.

Lee, Soyeon, e Kyung-Tai Min. «The Interface Between ER and Mitochondria: Molecular Compositions and Functions». Molecules and Cells 41, n. 12 (2018): 1000–1007. https://doi.org/10.14348/molcells.2018.0438.

Levraut, Jacques, Hirotaro Iwase, Z.-H. Shao, Terry L. Vanden Hoek, e Paul T. Schumacker. «Cell Death during Ischemia: Relationship to Mitochondrial Depolarization and ROS Generation». American Journal of Physiology. Heart and Circulatory Physiology 284, n. 2 (2003): H549-558.

Lin, M.T., and Beal, M.F. (2006). Mitochondrial dysfunction and oxidative stress in neurodegenerative diseases. Nature *443*, 787–795.

Lomas, DA, Evans DL, et al., (1992), The mechanism of Z alpha1- antitrypsin accumulation in the liver, *Nature*, 357(6379): 605-607.

Lomas, D.A., and Carrell, R.W. (2002). Serpinopathies and the conformational dementias. Nat. Rev. Genet. *3*, 759–768.

Lomas et al., (2016). Update on alpha1-antitrypsin deficiency:New therapies, Journal of Hepatology 2016 vol. 65 j 413–424.

Madani, R., Kozlov, S., Akhmedov, A., Cinelli, P., Kinter, J., Lipp, H.-P., Sonderegger, P., and Wolfer, D.P. (2003). Impaired explorative behavior and neophobia in genetically modified mice lacking or overexpressing the extracellular serine protease inhibitor neuroserpin. Molecular and Cellular Neuroscience *23*, 473–494.

Maharjan, S., Oku, M., Tsuda, M., Hoseki, J., and Sakai, Y. (2014). Mitochondrial impairment triggers cytosolic oxidative stress and cell death following proteasome inhibition. Sci Rep *4*, 5896.

Marcus, N.Y., Blomenkamp, K., Ahmad, M., and Teckman, J.H. (2012). Oxidative stress contributes to liver damage in a murine model of alpha-1-antitrypsin deficiency. Experimental Biology and Medicine *237*, 1163–1172.

Mayo, J.C., Tan, D.X., Sainz, R.M., Natarajan, M., Lopez-Burillo, S., and Reiter, R.J. (2003). Protection against oxidative protein damage induced by metal-catalyzed reaction or alkylperoxyl radicals: comparative effects of melatonin and other antioxidants. Biochim. Biophys. Acta *1620*, 139–150.

Miranda, E., Römisch, K., and Lomas, D.A. (2004). Mutants of neuroserpin that cause dementia accumulate as polymers within the endoplasmic reticulum. J. Biol. Chem. *279*, 28283–28291.

Mironov SL (2009) Complexity of mitochondrial dynamics in neurons and its control by ATP produced during synaptic activity.Int J Biochem Cell Biol. 2009 Oct;41(10):2005-14. doi: 10.1016/j.biocel.2009.04.009.

Moriconi, C., Ordoñez, A., Lupo, G., Gooptu, B., Irving, J.A., Noto, R., Martorana, V., Manno, M., Timpano, V., Guadagno, N.A., et al. (2015). Interactions between N-linked glycosylation and polymerisation of neuroserpin within the endoplasmic reticulum. FEBS J. *282*, 4565–4579.

Morinaka A, Yamada M, Itofusa R, Funato Y, Yoshimura Y, Nakamura F, Yoshimura T, Kaibuchi K, Goshima Y, Hoshino M, Kamiguchi H, Miki H. (2011). Thioredoxin mediates oxidation-dependent phosphorylation of CRMP2 and growth cone collapse. Sci Signal. Apr 26;4(170):ra26.

Munnamalai, Vidhya, e Daniel M. Suter. «Reactive Oxygen Species Regulate F-Actin Dynamics in Neuronal Growth Cones and Neurite Outgrowth». Journal of Neurochemistry 108, n. 3 (2009): 644–61.

Nicholls, D (2004). Mitochondrial membrane potential and aging. Aging Cell DOI: 10.1111/j.1474-9728.2003.00079

Oikawa, Shinji, Tomoko Yamada, Toshikazu Minohata, Hatasu Kobayashi, Ayako Furukawa, Saeko Tada- Oikawa, Yusuke Hiraku, Mariko Murata, Mitsuru Kikuchi, e Tetsumori Yamashima. Proteomic Identification of Carbonylated Proteins in the Monkey Hippocampus after Ischemia-

Reperfusion. Free Radical Biology & Medicine 46, n. 11 (2009):1472–77.

Okatani, Y., Wakatsuki, A., Reiter, R.J., Enzan, H., and Miyahara, Y. (2003). Protective effect of melatonin against mitochondrial injury induced by ischemia and reperfusion of rat liver. Eur. J. Pharmacol. *469*, 145–152.

Onorati, M., Binetti, M., Conti, L., Camnasio, S., Calabrese, G., Albieri, I., Di Febo, F., Toselli, M., Biella, G., Martynoga, B., et al. (2011). Preservation of positional identity in fetus-derived neural stem (NS) cells from different mouse central nervous system compartments. Cell. Mol. Life Sci. *68*, 1769–1783.

Potempa, J., E. Korzus, e J. Travis. «The Serpin Superfamily of Proteinase Inhibitors: Structure, Function, and Regulation». The Journal of Biological Chemistry 269, n. 23 (1994): 15957–60.

Reiter, R.J., Tan, D.X., Qi, W., Manchester, L.C., Karbownik, M., and Calvo, J.R. (2000). Pharmacology and physiology of melatonin in the reduction of oxidative stress in vivo. Biol Signals Recept *9*, 160–171.

Ricci, Jean-Ehrland, Roberta A. Gottlieb, e Douglas R. Green. Caspase-Mediated Loss of Mitochondrial Function and Generation of Reactive Oxygen Species during Apoptosis. The Journal of Cell Biology 160, n. 1 (2003): 65–75.

Roberts, A. W., Kim, C., Zhen, L., Lowe, J. B., Kapur, R., Petryniak, B., et al. (1999). Deficiency of the hematopoietic cell-specific Rho family GTPase Rac2 is characterised by abnormalities in neutrophil function and host defense. *Immunity* 10, 183–196. doi: 10.1016/s1074-7613(00)80019-9.

Roussel, B.D., Irving, J.A., Ekeowa, U.I., Belorgey, D., Haq, I., Ordóñez, A., Kruppa, A.J., Duvoix, A., Rashid, S.T., Crowther, D.C., et al. (2011). Unravelling the twists and turns of the serpinopathies. FEBS J. *278*, 3859–3867.

Roussel, B.D., Kruppa, A.J., Miranda, E., Crowther, D.C., Lomas, D.A., and Marciniak, S.J. (2013a). Endoplasmic reticulum dysfunction in neurological disease. The Lancet Neurology *12*, 105–118.

Roussel, B.D., Newton, T.M., Malzer, E., Simecek, N., Haq, I., Thomas, S.E., Burr, M.L., Lehner, P.J., Crowther, D.C., Marciniak, S.J., et al. (2013b). Sterol metabolism regulates neuroserpin polymer degradation in the absence of the unfolded protein response in the dementia FENIB. Human Molecular Genetics *22*, 4616–4626.

Roussel, B.D, Lomas DA, Crowther DC. Progressive myoclonus epilepsy associated with neuroserpin inclusion bodies (neuroserpinosis). (2016) Epileptic Disord. 2016 Sep 1;18 (S2):103-110.

Satoh, T., Y. Enokido, H. Aoshima, Y. Uchiyama, e H. Hatanaka. Changes in Mitochondrial Membrane Potential

during Oxidative Stress-Induced Apoptosis in PC12 Cells. Journal of Neuroscience Research 50, n. 3 (1997): 413–20.

Satoh, E., Okada, M., Takadera, T., and Ohyashiki, T. (2005). Glutathione Depletion Promotes Aluminum-Mediated Cell Death of PC12 Cells. Biological & Pharmaceutical Bulletin *28*, 941–946.

Soldati, C., Cacci E, Biagioni S, Carucci N, Lupo G, Perrone-Capano C, Saggio I, Augusti-Tocco G. (2012). Restriction of neural precursor ability to respond to Nurr1 by early regional specification. PLoS One 7(12): e51798.

Sveger T. Liver disease in alpha1-antitrypsin deficiency detected by screening of 200,000 infants. N Engl J Med 1976;294: 1316–1321.

Sharp HL, Bridges RA, Krivit W, and Freier EF, (1969), Cirrhosis associated with alpha-1-antitrypsin deficiency: A previously unrecognized inherited disorder, *J Lab Clin Med*, 73, 934-939

Trinczek, B., Ebneth, A., Mandelkow, E.M., and Mandelkow, E. (1999). Tau regulates the attachment/detachment but not the speed of motors in microtubule-dependent transport of single vesicles and organelles. J. Cell. Sci. *112 (Pt 14)*, 2355–2367.

Urata, Y., Honma, S., Goto, S., Todoroki, S., Iida, T., Cho, S., Honma, K., and Kondo, T. (1999). Melatonin induces gamma-glutamylcysteine synthetase mediated by activator protein-1 in

human vascular endothelial cells. Free Radic. Biol. Med. *27*, 838–847.

Wood-Kaczmar, Alison, Sonia Gandhi, Zhi Yao, Andrey S. Y. Abramov, Erik A. Miljan, Gregory Keen, Lee Stanyer, et al. PINK1 Is Necessary for Long Term Survival and Mitochondrial Function in Human Dopaminergic Neurons. A cura di Henry Waldvogel. PLoS ONE 3, n. 6 (2008): e2455. https://doi.org/10.1371/journal.pone.0002455.

Wu, Yumei, Christina Whiteus, C. Shan Xu, Kenneth J. Hayworth, Richard J. Weinberg, Harald F. Hess, e Pietro De Camilli. Contacts between the Endoplasmic Reticulum and Other Membranes in Neurons. Proceedings of the National Academy of Sciences of the United States of America 114, (13 2017): E4859–67.

Wilson and Gonzalez-Billault, (2015). Regulation of cytoskeletal dynamics by redox signaling and oxidative stress: implications for neuronal development and trafficking. Front Cell Neurosci 2015 Sep 30; 9:381.

Xiong J, Verkhratsky A, Toescu EC (2002) Changes in mitochon- drial status associated with altered Ca^{2+} homeostasis in aged cerebellar granule neurons in brain slices. *J. Neurosci.* 22, 10 761– 10 771.

Yamasaki M, Li W, Johnson DJ, Huntington JA, (2008), Crystal structure of a stable dimer reveals the molecular basis of serpin polymerisation, *Nature*, 455: 1255–1258.

Yamasaki M, Sendall TJ, Pearce MC, Whisstock JC, Huntington JA, (2011), Molecular basis of alpha (1)-antitrypsin deficiency revealed by the structure of a domain-swapped trimer, *EMBO Rep*, 12: 1011–1017.

Zakharova, I.O., Sokolova, T.V., Vlasova, Y.A., Bayunova, L.V., Rychkova, M.P., and Avrova, N.F. (2017). α-Tocopherol at Nanomolar Concentration Protects Cortical Neurons against Oxidative Stress. Int J Mol Sci *18*.

Zamzami N, Hirsch T, Dallaporta B, Petit PX, Kroemer G. (1997) Mitochondrial implication in accidental and programmed cell death: apoptosis and necrosis. J Bioenerg Biomembr 1997 Apr;29(2): 185-93.

Zhang, Y., and Chan, D.C. (2007). New insights into mitochondrial fusion. FEBS Lett. *581*, 2168–2173.

SECTION II

DISSECTING IMMUNOMODULATORY MECHANISMS OF A1AT WITH FUNCTION-NEUTRALISING MONOCLONAL ANTIBODIES

SUMMARY

Alpha-1 antitrypsin (A1AT) is a serine protease inhibitor predominantly synthesised in the liver. Its main function is to protect the extracellular matrix of the lung from excessive breakdown by neutrophil elastase. A1AT deficiency (A1ATD) is a genetic condition that predisposes to liver disease (neonatal hepatitis, cirrhosis, hepatocarcinoma) and destructive pulmonary inflammation (emphysema/COPD). The liver disease is predominantly associated with a toxic gain-of-function due to misfolding and polymerisation of mutant A1AT protein, while the lung disease is mainly due to loss of antiprotease function. Additionally, increasing data support multiple immunomodulatory roles for A1AT, probably independent from its anti-protease function. It is currently challenging to study how these immunomodulatory functions are mediated and to evaluate their significance in health and disease, mainly due to the lack of specific tools useful for cell culture assays. Monoclonal antibody (mAb)-mediated neutralization/modulation of functional activity is a well-established tool in immunological research that is currently lacking for the study of A1AT-mediated immunomodulation. In this project, we characterised a panel of mAbs, including newly produced and previously generated ones, and screened

them in *in vitro* model systems to identify mAbs that can selectively block the inhibitory and/or immunomodulatory effects of A1AT.

SOMMARIO

L'alpha-1 antitripsina (A1AT) è un inibitore di proteasi a serina sintetizzato principalmente a livello del fegato. La sua funzione principale è quella di proteggere la matrice extracellulare polmonare dall'azione dell'elastasi prodotta dai neurotrofili. Il deficit di A1AT (A1ATD) è una condizione genetica che predispone a patologie epatiche (epatite neonatale, cirrosi, epatocarcinoma) e infiammazioni a livello polmonare (enfisema/CODP). La malattia epatica è principalmente associata con l'acquisizione di funzione tossica data dalla polimerizzazione della proteina mutante A1AT. In vece, l'associata patologia polmonare è attribuita principalmente alla perdita della funzione anti-proteasica. Numerosi dati supportano anche un ruolo immunomodulatorio per l'A1AT, probabilmente indipendente dalla sua funzione anti-proteasica. Attualmente è difficile studiare come queste funzioni immunomodulatorie siano mediate e valutarne la relativa importanza in condizioni di salute e patologiche, principalmente per la mancanza di reagenti adatti alla ricerca in modelli di coltura cellulare.

La modulazione/neutralizzazione mediata da anticorpi monoclonali (mAbs) è uno strumento altamente delineato nella ricerca immunologica, che attualmente non è stato ancora utilizzato nello studio dell'immunomodulazione mediata dall'A1AT. In questo progetto abbiamo caratterizzato un

panello di anticorpi preesistenti e di nuova generazione su modelli *in vitro* allo scopo d'identificare quali possono bloccare selettivamente la funzione inibitoria e/o gli effetti immunomodulatori dell'A1AT.

Introduction

Alpha-1 antitrypsin (A1AT) is synthesized by the liver and is the most abundant circulating protease inhibitor. It functions primarily as an inhibitor of the enzyme neutrophil elastase in the lungs. Most individuals are homozygous for the wild type M allele, with the commonest deficiency alleles being the severe Z (Glu342Lys) and the mild S (Glu264Val) variants (Gooptu et al., 2014). These mutations induce the protein to be degraded by endoplasmic reticulum (ER)-associated degradation (ERAD) and to form ordered polymers that are retained within the ER of hepatocytes, forming periodic acid-Schiff (PAS) positive, diastase resistant inclusions (Lomas et al., 1992). These inclusions are associated with neonatal hepatitis, cirrhosis and hepatocellular carcinoma (Sveger et al., 1976; Eriksson et al., 1986). Only 10-15% of Z A1AT is folded and released into the circulation, leaving the lungs exposed to enzymatic damage by neutrophil elastase and so predisposing the Z homozygote to early onset lobular emphysema. The S allele results in less retention of protein within hepatocytes, with plasma levels reaching 60% of those of the M allele. A1AT is also a liver-derived acute phase protein that, *in vitro* and *in vivo*, reduces production of pro-inflammatory cytokines, inhibits apoptosis, blocks leukocyte degranulation and migration, and modulates local and systemic inflammatory responses (Ehlers, 2014). The immunomodulatory functions of A1AT have long been recognized, with the most studied effects on neutrophilic inflammation (Bergin et al., 2014; Mahadeva et al., 2005). Native A1AT is considered an anti-inflammatory protein, while its polymers have pro-inflammatory effects upon

neutrophils *in vitro* and *in vivo* (Mahadeva et al., 2005). Many studies now support immunomodulatory roles for native A1AT in several contexts, from airway epithelial cells (Van't Wout et al., 2013) to peripheral blood mononuclear cells (PBMCs) (Janciauskiene et al., 2007). The mechanisms by which these roles are mediated are unclear. Some proposed immunomodulatory effects depend upon antiprotease functions of A1AT. Inhibition of elastase activity may modulate inflammation by several mechanisms, which include preventing chemotaxis due to elastin degradation products (Senior et al., 1980; Houghton et al., 2006) or due to macrophage stimulation by free elastase (Hubbard et al., 1991); preventing PAR-1 (protease activated receptor 1) activation (Suzuki et al., 2005, 2009); and preventing release/activation of cytokines (Taipale et al., 1995; Lefracais et al., 2012). Other antiprotease activities of A1AT may underlie different immunomodulatory effects. For example, loss of anti-proteinase 3 (PR3) A1AT function may be more important than previously recognized in A1ATD (Sinden et al., 2013, 2015). PR3 inhibition down-regulates activation of IL (interleukin)-32 produced by natural killer and stimulated T lymphocytes (Marcondes et al., 2011). A1AT treatment also prevents cell surface PR3 from binding to anti-PR3 autoantibodies, a pathogenic event in vasculitis and granulomatosis with polyangiitis (Surmiak et al., 2016). Interestingly, antiprotease-independent mechanisms are also supported by *in vitro* and clinical data (Morris et al., 2011). These include IL-8 binding (Bergin et al., 2010); TNF (tumor necrosis factor)-α receptor binding, and IL-10 induction in $CD4^{+}$T lymphocytes (Bergin et al., 2014). In some cases, both antiprotease-dependent and -independent mechanisms may

contribute in parallel, such as LPS (lipopolysaccharides)-mediated effects on mouse lung (Jonigk et al., 2013). In most cases the mechanistic relationship of the immune modulation to antiprotease function in A1ATD is entirely unknown. Immunomodulatory effects with uncharacterized mechanism include the modulation of TNF-α responses from endothelial cells (Lockett et al., 2013); biphasic effects of A1AT in LPS-induced airway inflammation (Subramaniyam et al., 2010; Nita et al., 2005); reducing neutrophil migration in response to LPS challenge (Jonigk et al., 2013); and stimulation of anti-inflammatory IL-1RA secretion from monocytes (Tilg et al., 1993). In the last case, the mechanism(s) by which these potentially important immunomodulatory roles are exerted remain largely uncharacterized. The relative significance of all the proposed immunomodulatory roles *in vivo* remains minimally quantified. However, it is currently difficult to study how these immunomodulatory functions are mediated and to evaluate the contribution of these regulatory mechanisms in health or their loss in disease. The use of functional monoclonal antibodies (mAbs) to neutralize or modulate a protein's activity is a well-established tool in immunological research but is still lacking for the study of A1AT-mediated immunomodulation. In this part of my thesis, which was funded by the Alpha-1 Foundation (USA) and developed as a collaboration with Juan Perez from the University of Malaga (Spain) and Catherine Hawrylowicz from King's College London (UK), we set up to identify anti-A1AT monoclonal antibodies able to block the immunomodularory effects of A1AT and/or its anti-proteinase activity, by generating new mAbs against M A1AT and

screening them, together with previously generated ones, in several *in vitro* assays (ELISA, primary human cell culture).

Results

Mouse immunisation

The immunisation for generating new mAbs against wild type M A1AT was carried out by Prof. Juan Perez, at University of Malaga (Spain). The immunogen consisted in native, active M A1AT purified from human plasma (0.81 mg/ml) provided by our collaborators at University College London (UK), mixed with complete (first dose) or incomplete (boosters) Freud's adjuvant. Ten female Balb/C mice of 8 weeks of age were injected with the immunogen, five of them received 15 µg A1AT/dose (high dose) and the other five 7,5 µg A1AT/dose (low dose), in the first (priming) and following four (booster) injections (Fig 1). Three days after the final boost (performed with the antigen in PBS only), spleen cells and corresponding immune sera were pooled in four aliquots [mice 1+2 (low dose), 3+4 (low dose), 5+6 (high dose) and 7+8 (high dose)], frozen and kept in liquid N_2 until they were used for the fusion.

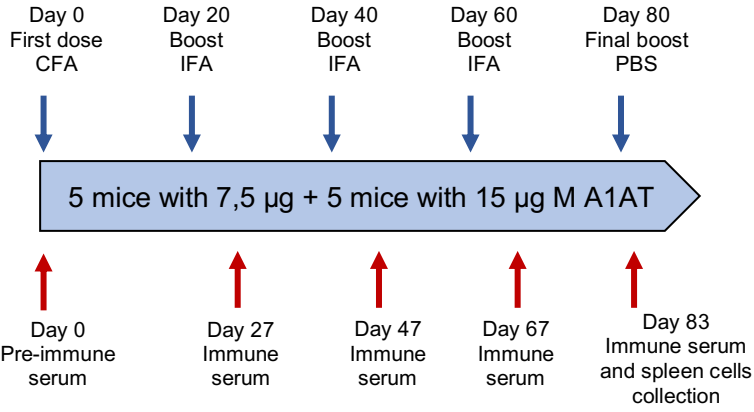

Figure 1. Timetable of anti-M A1AT immunization. The immunisation was done with active M A1AT purified from human plasma. Ten female mice Balb/C of 8 weeks of age were injected with the immunogen, five of the ten mice received 15 µg/dose (high dose) and the other five 7,5 µg/dose (low dose), in the first (priming) and subsequent (booster) injections. CFA: complete Freud's adjuvant; IFA: incomplete Freud's adjuvant.

Testing of the immune sera

The sera of immunised mice were analysed by antigen ELISA, coating the plates with M A1AT at a final concentration of 2 µg/ml. The immune sera were pooled in the same order used for the spleen cells (mice 1+2, 3+4, 5+6 and 7+8), and were analysed starting from a 1:1000 dilution in blocking buffer with sequential 1:2 dilutions. As shown in figure 2, pools 3+4 and 5+6 seemed to have slightly higher titles than the other two pools. For comparison, the immune sera from 2008 (generation of mAbs against polymeric Z A1AT) and 2010 (generation of mAbs against monomeric Z A1AT) were tested in parallel, as well as a negative control non-immune mouse serum.

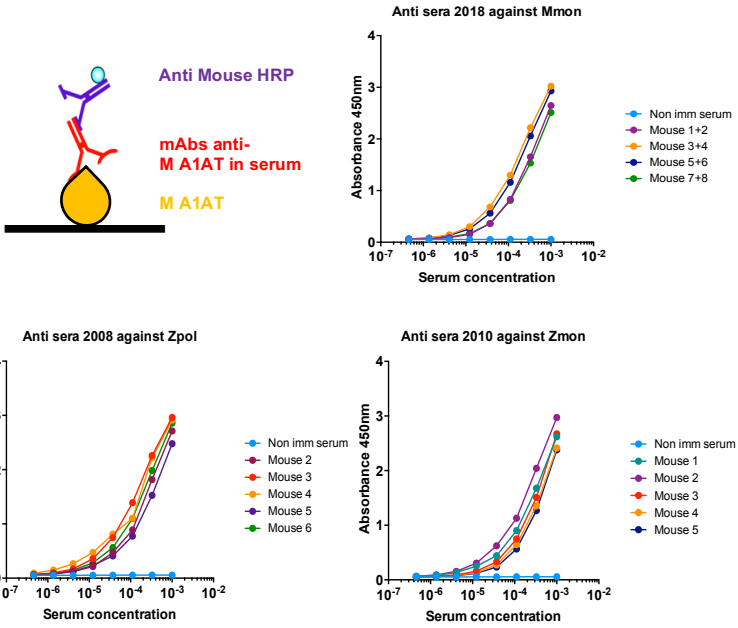

Figure 2. Testing of immune sera by antigen ELISA. The immune sera of mice immunised with M A1AT (Mmon) were pooled (mice 1+2, 3+4, 5+6 and 7+8) and tried in antigen ELISA starting from 1:1000 dilution and with sequential 1:2 dilutions. For comparison, the immune sera from 2008 (anti-Z A1AT polymer, Zpol) and 2010 (anti-Z A1AT monomer, Zmon) were tested in parallel.

Production of hybridoma cells and screening for positive hybrids

Cell fusion was performed using the spleen cells from mice immunized with M A1AT and mouse myeloma cells (P3-X63-Ag.8.653). For each fusion, spleen cells were thawed in DMEM-20, washed once with DMEM and counted; myeloma cells were washed twice with DMEM and counted; when ready, both two cell types were mixed at a 1 (spleen) +3 (myeloma) proportion and fused by using the polyethylene glycol method (see Methods). One pool of cells from two spleens (prepared as described above) was used for each fusion, and all four pools were used. Hybridoma growth was poor after fusions 1 and 2, and normal for fusions 3 and 4. A total of nearly 1500 wells were screened for anti-M A1AT antibodies after seven days of growth, using the antigen ELISA format (coating the plates with M A1AT at 2 μg/ml). The proportion of positive wells was very low, suggesting that the immunisation with human wild type M A1AT stimulated

the mouse immune system only poorly. Positive wells from fusion plates were expanded in 24-well plates, checked again for positivity after expansion, and cloned by diagonal dilution (see Methods). The new lines obtained were named 2D4, 2G5, 3G7 and 3F7, according to the plate number and well position for each of the original hybridoma wells.

ELISA characterisation of anti-M A1AT mAbs affinity for different A1AT conformers

The new anti-M A1AT mAbs were tested by antigen ELISA using M monomer, Z monomer and Z polymer as antigens, coating the plates at 2 μg/ml, and using hybridoma culture medium supernatant (CMS) starting from 1:1 and with 1:3 serial dilutions. The anti-Z monomer mAb 3C11, which recognises all conformers of M and Z A1AT with similar affinities (Tan et al., 2015), was included for comparison (Fig. 3). In this ELISA, 2D4 and 2G5 showed the highest signals, with similar affinities for all three antigens.

The new mAbs were also tested by sandwich ELISA (Fig. 4), using a rabbit polyclonal antibody against M A1AT for capture and M monomer, Z monomer and Z polymers as antigens, starting from 1 μg/ml with 1:3 serial dilutions of the antigen. MAbs were used as CMS diluted to a fixed concentration of 1:100 in blocking buffer for mAbs 2G5 and 2D4 and the positive control 3C11, since they showed the highest signals in antigen ELISA; and 1:50 for mAbs 3G7 and 3F7, and also for the Z A1AT polymer-specific mAb 2C1 used here for comparison. Unexpectedly, mAbs 2D4 and particularly 2G5, and to variable degrees the remaining mAbs in the different antigens, showed a remarkable loss of signal in this sandwich ELISA.

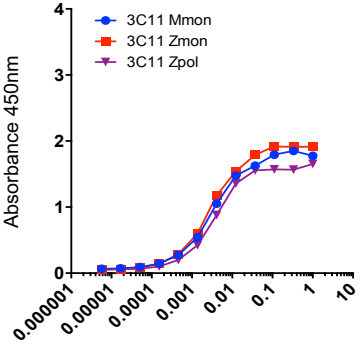
3C11 Mmon
3C11 Zmon
3C11 Zpol
Absorbance 450nm
0
1
2
3
4
0.000001
0.00001
0.0001
0.001
0.01
0.1
1
10

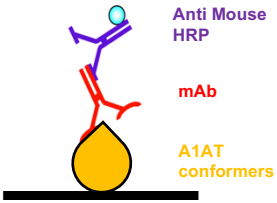
Anti Mouse
HRP
mAb
A1AT
conformers

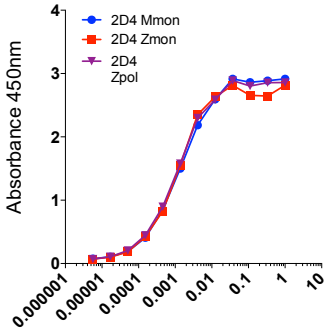
2D4 Mmon
2D4 Zmon
2D4
Zpol
Absorbance 450nm
0
1
2
3
4
0.000001
0.00001
0.0001
0.001
0.01
0.1
1
10

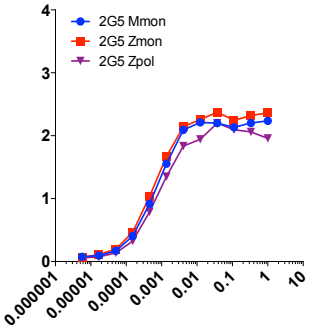
2G5 Mmon
2G5 Zmon
2G5 Zpol
0
1
2
3
4
0.000001
0.00001
0.0001
0.001
0.01
0.1
1
10

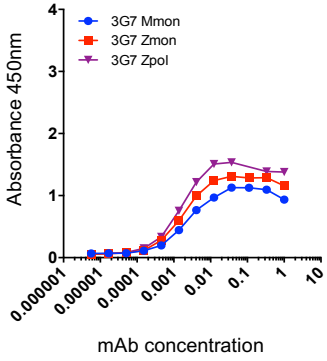
3G7 Mmon
3G7 Zmon
3G7 Zpol
Absorbance 450nm
0
1
2
3
4
0.000001
0.00001
0.0001
0.001
0.01
0.1
1
10
mAb concentration

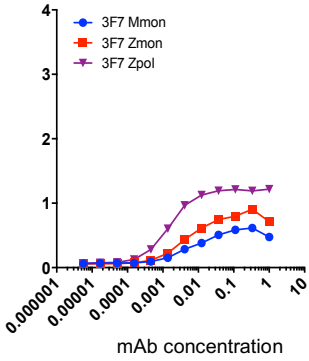
3F7 Mmon
3F7 Zmon
3F7 Zpol
0
1
2
3
4
0.000001
0.00001
0.0001
0.001
0.01
0.1
1
10
mAb concentration

Figure 3. Testing of anti-M A1AT mAbs by antigen ELISA. ELISA plates were coated with M monomer, Z monomer or Z polymer A1AT at 2 μg/ml. The culture medium supernatants were tried starting from 1:1 and with sequential 1:3 serial dilutions. For comparison, mAb 3C11 (produced in 2010 and with high affinity for all A1AT conformers) was included as a control.

A

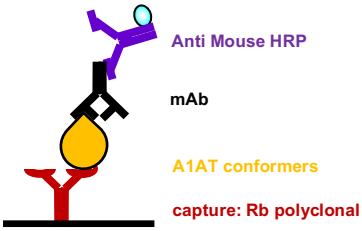

B

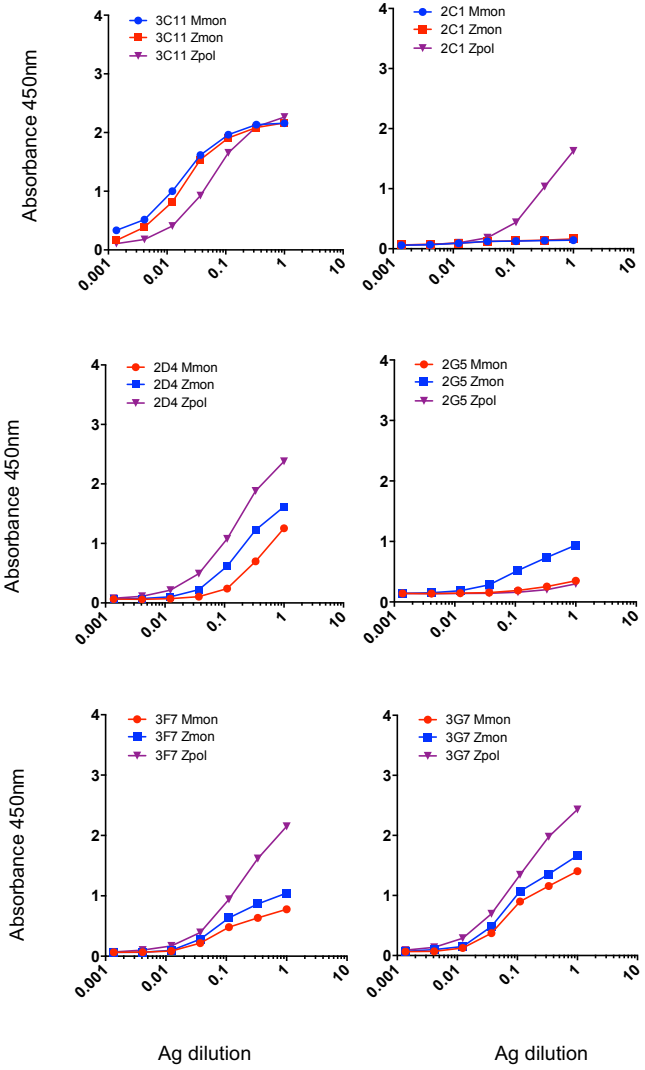
3C11 Mmon
3C11 Zmon
3C11 Zpol
2C1 Mmon
2C1 Zmon
2C1 Zpol
2D4 Mmon
2D4 Zmon
2D4 Zpol
2G5 Mmon
2G5 Zmon
2G5 Zpol
3F7 Mmon
3F7 Zmon
3F7 Zpol
3G7 Mmon
3G7 Zmon
3G7 Zpol
Absorbance 450nm
Absorbance 450nm
Absorbance 450nm
0
1
2
3
4
0.001
0.01
0.1
1
10
Ag dilution
Ag dilution

Figure 4. Testing of anti-M A1AT mAbs by sandwich ELISA. **A.** Schematic representation of the elastase sandwich ELISA. **B.** ELISA plates were coated with purified rabbit anti-M A1AT polyclonal antibody, followed by incubation with M monomer, Z monomer or Z polymer AAT starting from 1 μg/ml and fixed concentrations of the mAbs (CMS 1:100 for 3C11, 2D4 and 2G5; CMS 1:50 for 2C1, 3F7 and 3G7). For comparison, mAbs 3C11 and 2C1 (Miranda et al., 2010, polymer-specific) were included as controls.

Selection of a mAb panel for the screening of functional mAbs

In view of the reduced number of mAbs obtained from the immunisation with M A1AT, we decided to expand the panel of mAbs for our studies by selecting other hybridoma lines obtained in previous immunisation campaigns (performed in 2008, 2010 and 2017). We thus created a panel of 19 different mAbs to be tested in our secondary screening for mAbs able to block the inhibitory activity of A1AT and/or able to modify the immunomodulatory properties of M AAT in PBMC cultures. The full list of mAbs selected for trial in this secondary screening, selected for having a high affinity for M A1AT or for all A1AT conformers, is shown in Table 1.

	Mab	Year of production	Conformers specificity
against monomeric M A1AT	2D4	2018	high affinity for all A1AT conformers
	2G5		high affinity for all A1AT conformers
	3G7		medium affinity for all A1AT conformers
	3F7		medium affinity for all A1AT conformers
against M and Z A1AT polymers	1D9	2017	high affinity for monomeric A1AT
	6B4		high affinity for M A1AT
	2H2		high affinity for monomeric A1AT
	8A7		high affinity for all A1AT conformers
	10C8		high affinity for all A1AT conformers
	1D12		high affinity for all A1AT conformers
	1A1		high affinity for all A1AT conformers
	1H2		high affinity for all A1AT conformers
against monomeric Z A1AT	2F4	2011	high affinity for all A1AT conformers
	4B12		high affinity for all A1AT conformers, polymerisation blocking mAb (Ordoñez et al, 2015)
	3C11		high affinity for all A1AT conformers
against Polymers of Z A1AT	9C5	2008	high affinity for all A1AT conformers
	7H2		good affinity for all A1AT conformers
	2A2		good affinity for all A1AT conformers
	7B5		good affinity for all A1AT conformers

Table 1. Complete panel of mAbs selected. Panel of mAbs used for secondary screening of antibodies with

A1AT function-modifying activity. Listed mAbs were obtained in the current and previous immunisation campaigns (unpublished and Miranda et al., 2010; Ordoñez et al., 2015; Tan et al., 2015).

Secondary screening for mAbs that block A1AT-elastase complex formation

This secondary screening was aimed to detecting mAbs able to prevent complex formation between M A1AT and elastase, using a novel ELISA assay (elastase ELISA) devised for this aim, based on coating the plates with purified, active M A1AT, promoting complex formation with elastase in the absence or presence of the mAbs to be tried, and quantifying complex formation with an anti-elastase antibody (see Methods). This assay was able to detect complex formation with a maximum signal of approximately 1.4 a.u. (absorbance at 450 nm). We used this ELISA to screen CMS from all the hybridomas listed in table 1. The only mAb able to cause a small reduction in signal (of approx. 0.4 units) was 3C11, an anti-Z monomer mAb produced in 2010. In an effort to understand if our immunisation strategy was appropriated for producing mAbs able of blocking inhibitory activity, we also tested the anti-M AAT immune sera (2018) in this elastase ELISA, and for comparison the immune sera corresponding to anti-Z A1AT monomer mAbs (2010) and anti-Z A1AT polymer mAbs (2008). The results are shown in figure 5. All four anti-M A1AT immune sera were able to decrease elastase complex formation to a similar degree, with a dose-dependent

effect, and generally better than sera produced in previous immunization campaigns. Out of the five sera produced against Z A1AT polymers in 2008, the one from mouse 4 was the most effective, while mice 2 and 3 were the most effective out of the five mice immunized in 2010.

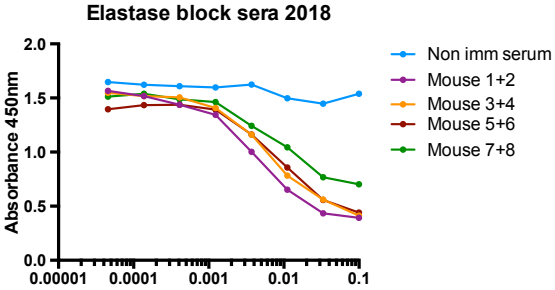
Elastase block sera 2018
Absorbance 450nm
2.0
1.5
1.0
0.5
0.0
0.00001
0.0001
0.001
0.01
0.1
Non imm serum
Mouse 1+2
Mouse 3+4
Mouse 5+6
Mouse 7+8

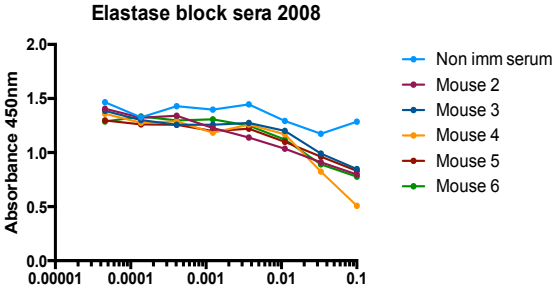
Elastase block sera 2008
Absorbance 450nm
2.0
1.5
1.0
0.5
0.0
0.00001
0.0001
0.001
0.01
0.1
Non imm serum
Mouse 2
Mouse 3
Mouse 4
Mouse 5
Mouse 6

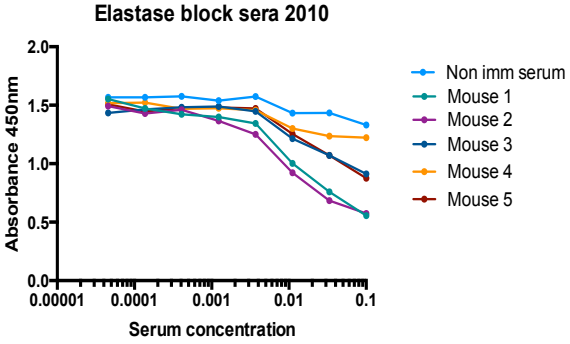
Elastase block sera 2010
Absorbance 450nm
2.0
1.5
1.0
0.5
0.0
0.00001
0.0001
0.001
0.01
0.1
Serum concentration
Non imm serum
Mouse 1
Mouse 2
Mouse 3
Mouse 4
Mouse 5

Figure 5. Testing of immune sera in the elastase ELISA. The immune sera produced against M A1AT (2018) were tested in elastase ELISA assay, as well as those against anti-Z A1AT monomer (2010) and anti-Z A1AT polymers (2008) for comparison.

In order to improve the detection of A1AT function-blocking antibodies, we developed an alternative format for the elastase ELISA (Fig. 6A), by coating the plate with purified mAb 9C5 (Miranda et al., 2010, a mAb that binds all A1AT conformers with good affinity), which captures M A1AT by binding to its single epitope, with the logic that this capture may preserve the native structure of A1AT better than the direct covalent binding to the ELISA plate. With this format, mAb 1D9 caused a clear, dose-dependent reduction in complex formation, while mAb 3C11 did not have any effect, with similar signals to our negative controls: a non-specific mAb (1A10, against neuroserpin) and blocking buffer with no mAb (Fig. 6). We thus re-tested all mAbs with the new ELISA (Fig. 7 and confirmed a reduction in elastase-A1AT complex formation with mAb 1D9, with no other hybridoma CMS having effect when compared to the negative control mAb 1A10. For completeness, we also re-tested the best and less performing immune sera of each immunisation campaign as seen with the first elastase assay and found similar results by using the 9C5-capture elastase sandwich ELISA (Fig. 8).

A

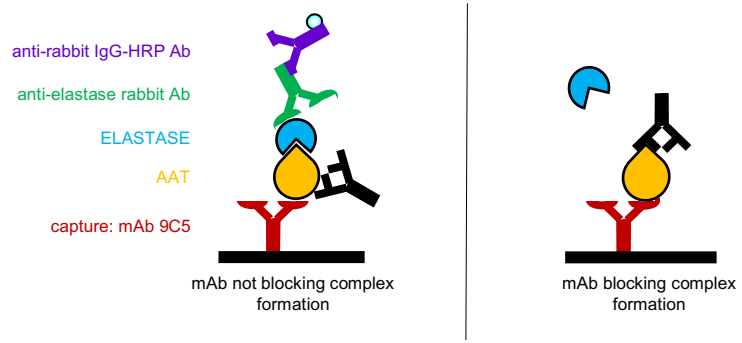

B

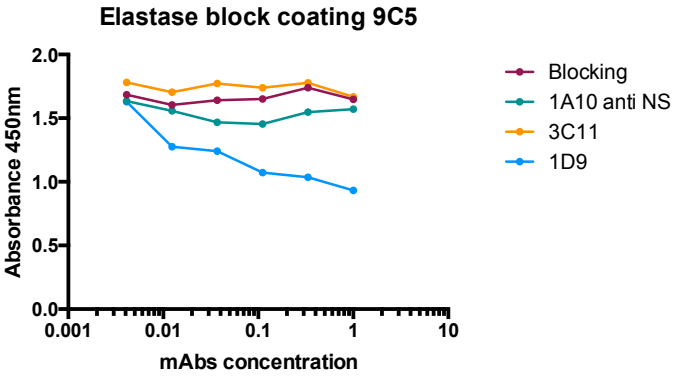

Figure 6. Elastase sandwich ELISA testing of selected mAbs. A. Schematic representation of the elastase sandwich ELISA. **B.** MAbs 3C11 and 1D9 were tried in the elastase sandwich ELISA using mAb 9C5 as a capture antibody, and the non-related anti-neuroserpin mAb 1A10 and blocking buffer only as negative controls.

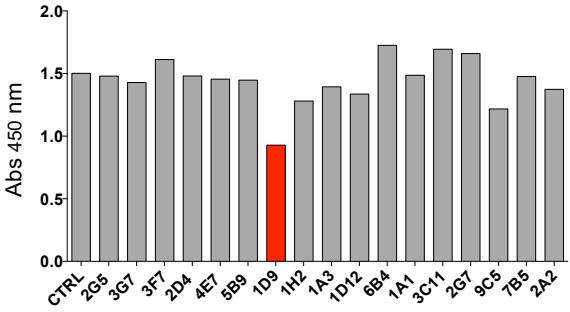

Figure 7. Elastase sandwich ELISA screening of all candidate mAbs. Using 9C5 for capturing M A1AT, candidate mAbs were tested as CMS for their ability to reduce A1AT-elastase complex formation. Compared to the anti-neuroserpin 1A10 negative control (CTRL), the candidate mAbs had a range of behaviours, with 1D9 causing a clear inhibition.

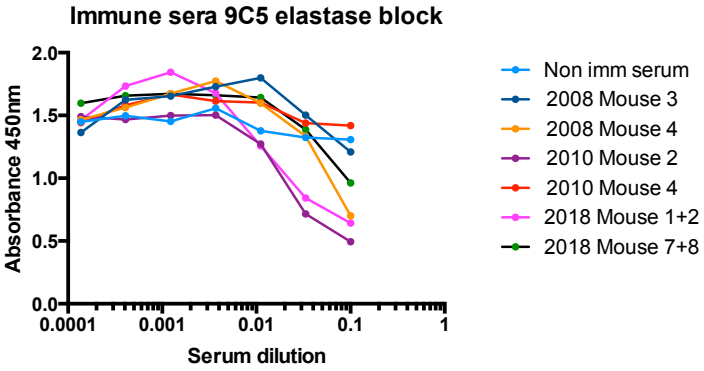

Figure 8. Testing of selected anti-A1AT immune sera in the elastase sandwich ELISA. Immune sera selected as the best and worst performing ones for each immunization campaign were tested in the new ELISA format.

Secondary screening for mAbs that block A1AT-PR3 complex formation

The equivalent ELISA for detection of M A1AT-PR3 complex formation did not perform well, due to a strong cross-reaction of the anti-PR3 antibody (Abcam ab21592) against M A1AT. An alternative anti-PR3 antibody (Abcam ab103632) was tested, but it gave a very low signal in ELISA, which precluded its use. To bypass this problem, we devised a

different ELISA format (Fig. 9), coating the plate with PR3 at 10 µg/ml, promoting complex formation with A1AT previously bound to the candidate mAbs, and using an anti-mouse-HRP antibody for quantification of complex formation. This PR3 ELISA showed a strong interference due to the bovine A1AT contained in the FBS of the CMS from the candidate hybridoma lines, which was able to form a complex with PR3 but was not bound by our mAbs (raised against human A1AT), causing a decrease in signal that precluded this secondary screening using CMS.

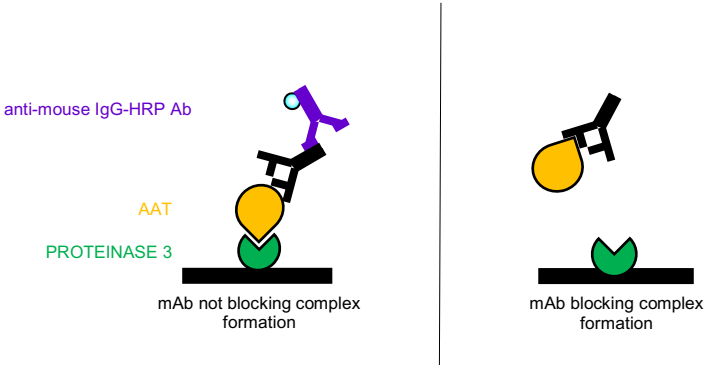

Figure 9. PR3 ELISA assay. Schematic representation of the ELISA assay for quantification of the PR3-M A1AT complex.

Purification of selected anti-A1AT mAbs

In order to better understand the properties of our mAbs, we decided to purify the best candidates so they could be tried as pure reagents, without interference from FBS and used at controlled concentrations. Purification of mAbs was performed using CMS collected from the hybridoma cell lines by affinity chromatography using HiTrap Protein G Sepharose columns. The source of mAb for purification is usually low serum CMS (1.25% FBS in culture medium specifically formulated to be used without serum) or regular DMEM supplemented with ultra-low IgG FBS, to avoid co-purification of bovine IgG from FBS. We opted for the second option, using DMEM-10% ultra-low IgG FBS. We ran 500 ml of each CMS at a maximum rate of 1 ml/min using a peristaltic pump overnight at RT and washed and eluted the column following the manufacturer's instructions (see Methods). We purified the most interesting antibodies for testing them in our *in vitro* assays as well as in peripheral blood mononuclear cells (PBMC) cultures: 1D9, 2H2, 6B4, 1D12, 2F4, 7H2, 2A2. The amounts of purified IgG obtained for each hybridoma line are presented in Table 2. After purification, all mAbs were dialysed against PBS overnight at 4°C, aliquoted and kept frozen at -20°C.

mAb	IgG purified (mg)
1D9	2,1 mg
2H2	0,1 mg
6B4	0,54 mg
1D12	1,81 mg
2F4	1,9 mg
7H2	0,8 mg
2A2	1,1 mg

Table 2. Amounts of purified IgG obtained for each hybridoma line after dialysation against PBS.

Purified mAb 1D9 inhibits complex formation between A1AT and elastase in a dose-dependent manner

We reassessed the properties of our best candidate mAbs as purified reagents, including 1D9 and other mAbs that showed weaker effects in our initial screening for antibodies able to block complex formation between A1AT and elastase using CMS from hybridoma cultures. As shown in figure 10A, mAb 1D9 was the only one able to reduce complex formation, doing so by more than 60% and in a dose-dependent manner (Fig. 10B). In our screening, we also observed a significant increase in elastase complex formation in the presence of mAb 4B12, a mAb that we reported in the past as able to prevent intracellular polymerisation of Z A1AT (Ordoñez et al., 2015).

A

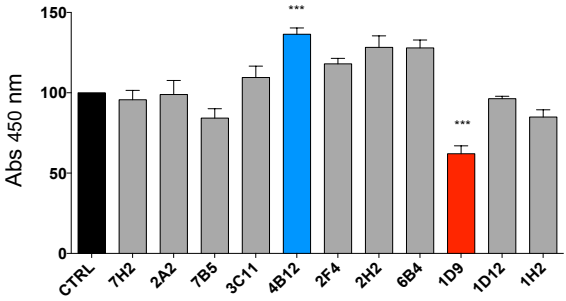

B

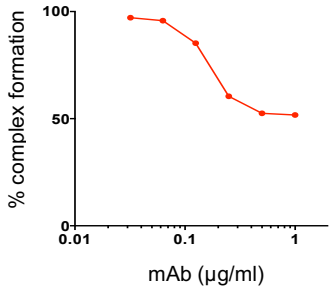

Figure 10. 1D9 decreases elastase-M A1AT complex formation. A. Testing of purified mAbs in the elastase sandwich ELISA using the mAbs at a fixed concentration of 10 µg/ml. **B.** Dose-response of the reduction in complex formation caused by mAb 1D9, starting from 1 µg/ml and with 1:3 dilutions. n = 3; t-test: ***p ≤ 0.001.

Secondary screening of purified mAbs for blocking of PR3-M A1AT complex formation

To avoid the problems due to the presence of FBS in the CMS as explained above, we tested our selected candidate mAbs as purified IgG in the PR3 ELISA assay. Our results show that only mAb 1D9 caused a reduction of A1AT-PR3 complex formation to levels equivalent to the negative control, in which the anti-neuroserpin mAb 1A10 does not bind to A1AT and so complex formation cannot be detected (see Fig. 9 for a diagram of this ELISA assay). Unexpectedly, mAb 4B12 caused a strong increase in signal in this assay.

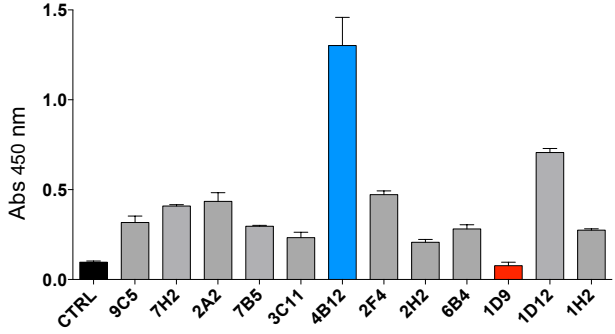

Figure 11. PR3 ELISA screening of purified candidate mAbs. Purified mAbs were tested in the PR3 ELISA assay described in figure 8. Negative control (CTRL) is anti-neuroserpin mAb 1A10, which does not bind A1AT and hence gives background signal only.

MAb 1D9 blocks heat-induced polymerisation of Z A1AT

Since the epitope of mAb 1D9 includes the reactive centre loop of A1AT (James Irving, University College London, UK, personal communication), we also tested the ability of this antibody to interfere with heat-induced polymerisation of Z AAT. We incubated Z A1AT purified from plasma at 0.4 mg/ml in PBS with decreasing amounts of mAb 1D9 (1.2, 0.5 and 0.2 mg/ml) or the polymerisation blocking mAb 4B12 (Ordoñez et al., 2015) as a reference, at 45°C for 45 h. The resulting mix was analysed by sandwich ELISA to quantify the amount of polymer formation, using a rabbit polyclonal anti-A1AT for capture and the polymer-specific 2C1 mAb conjugated to HRP for detection. As shown in figure 12, mAb 1D9 was able to reduce polymer formation in a dose-dependent manner.

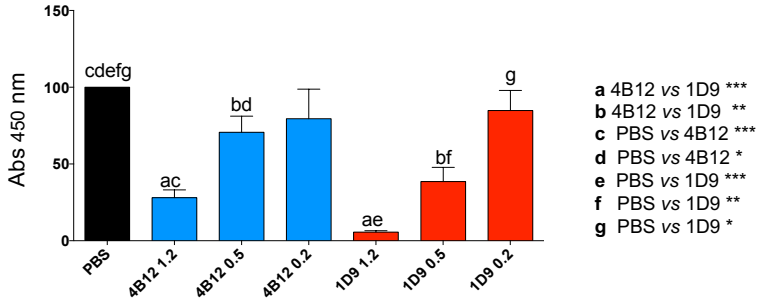

Figure 12. Test of interference with the heat-driven polymerisation of Z A1AT. Z A1AT purified from plasma was incubated at 0.4 mg/ml with three different amounts (1.2, 0.5 and 0.2 mg/ml) of mAb 1D9 or the polymerisation blocking mAb 4B12 as a reference (Ordoñez et al., 2015), and the resulting Z A1AT polymers were quantified by sandwich ELISA. n = 3; t-test: ***p ≤ 0.001, **p ≤ 0.01, *p ≤ 0.05.

MAbs 1D9 and 9C5 cause a decrease in IL-10 secretion in PBMC cultures

As part of our secondary screening, we also aimed to identify mAbs able to influence an immunomodulatory function of M A1AT, the induction of IL-10 secretion from PBMCs. This was carried on during my collaborative stage in the laboratory of Prof. Catherine Hawrylowicz, at King's College London (UK). Initially, PBMCs were treated with A1AT in the absence or presence of each candidate mAb supplied as CMS. After 24 h, the culture media and cell pellets from these cultures were collected for analysis. The culture media were analysed by CBA (colorimetric bead assay) to quantify IL-10 secretion (Fig. 13A), but the results were inconclusive due to the lack of immunomodulatory activity of the A1AT batch used, which did not show the expected increase in IL-10 secretion in the control well treated with A1AT only. The cell pellets were processed for RNA extraction, production of cDNA and qRT-PCR, in order to check expression levels of IL-1ra, a second marker of the immunomodulatory effect of A1AT in PBMCs. Again, the positive control well treated with A1AT only failed to show an increase in IL-1ra levels, so the mAb- treated samples were not analysed.

Several of the candidate mAbs, considered as the most promising due to their properties in other *in vitro* assays, were also tested as purified IgG. PBMC cultures were treated with M A1AT and each purified mAb at equimolecular concentrations, in triplicate wells for each mAb. After 24 h, the culture media were collected and used for IL-10 determination by CBA assay. Although the A1AT control failed again, not triggering the expected increase in IL-10

secretion, it is interesting to note that mAbs 1D9 and 9C5 caused a strong decrease in basal IL-10 levels (Fig. 13B). This experiment is currently being repeated by the Hawrylowicz lab with a fresh batch of A1AT.

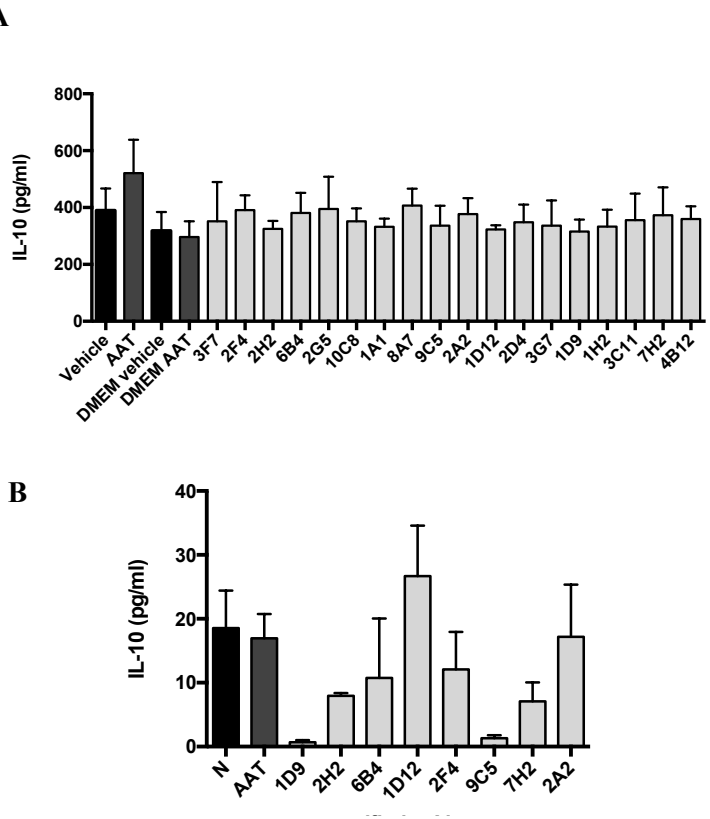

Figure 13. Testing of mAbs in PMBC cultures. A. Cultures of PBMCs were treated with A1AT alone (A1AT, 125 µg/ml) or in combination with each candidate mAb (as 250 µl of hybridoma CMS containing 20%

FBS). After 24 h, CMS were collected for analysis of IL-10 levels. **B.** Cultures of PBMC were treated with A1AT alone (A1AT, 125 µg/ml) or in combination with each purified mAb (187.5 µg). After 24 h, CMS were collected for analysis of IL-10 levels.

Discussion

The longest-recognised function of A1AT is to protect the lung tissue from excessive breakdown by neutrophil elastase, but a variety of immunomodulatory roles have now been assigned to this protein: many studies indicate immunomodulatory roles of native A1AT from airway epithelial cells (Van't Wout et al., 2013) to peripheral blood mononuclear cells (PBMCs) (Janciauskiene et al, 2007). The mechanisms by which these immunomodulatory roles are mediated are unclear. Our overall hypothesis is that a mAb, by binding specifically and with high affinity to its epitope in A1AT, can neutralize or even enhance an antiprotease and/or immunomodulatory function of human wild type (M) A1AT, which would advance our understanding of its anti-inflammatory roles and clarify the relevance of loss of these functions in disease. Our ELISA analysis of the sera of mice immunised with active, human M A1AT showed that there was an immune response against the protein, and that the immune sera contained anti-M A1AT antibodies able of reducing complex formation between A1AT and elastase, with one high-dose and one low-dose pool of sera showing a slightly better performance. In comparison to previous mAb production campaigns, the antisera produced in 2018 presented more consistent inhibitory-neutralisation properties, although a similar level of activity was shown by the best performing sera produced in 2008 and 2010. Unexpectedly, these results did not translate in the generation of numerous new hybridoma lines, as was expected from our previous experience (usually 10 to 20 new lines per fusion). Instead, the proportion of positive hybridoma wells after fusion with

myeloma cells was very low, suggesting that the immunisation with M A1AT was not as effective as initially thought. Our interpretation of these results is that M A1AT gave rise to a few high-affinity antibody clones against a handful of epitopes in human M A1AT able to stimulate the mouse immune system. These antibodies were enough to give a good signal in the ELISA testing the immune sera but gave rise to just a few new hybridoma lines after four fusion processes. Characterisation of the new lines by antigen ELISA showed a good affinity for M and Z A1AT in the monomeric and polymeric states, particularly high for mAbs 2D4 and 2G5. In contrast, the performance of these mAbs in sandwich ELISA, using the same antigens, was much poorer. This is probably due to a competition for antigen binding between the new mAbs and the rabbit polyclonal anti-M A1AT antibody used in the capture step, if the same epitopes are responsible for the immune response against human M A1AT in mouse and rabbit. In fact, this competition has not been observed before for other mAbs generated against the polymerogenic Z A1AT variant that probably presents different epitopes when compared to the wild type protein.

In view of the reduced number of mAbs obtained from our immunisation with M A1AT, we decided to expand the panel of mAbs to be tested for their ability to modify complex formation and/or immunomodulatory activity by selecting several mAbs obtained in previous years (Table 1), including antibodies generated against Z A1AT polymers, Z A1AT monomer and mixed M/Z A1AT polymers. To test the interference of candidate mAbs with complex formation between A1AT and its protease targets, we have developed

novel ELISA assays that allow us to screen many antibodies in a plate format and which may be applied in future studies similar to this one. We found that only mAb 1D9 is able to prevent complex formation between A1AT and elastase, both when used as CMS and as a purified IgG. This effect was only visible when A1AT was bound to the plate through capture by a different mAb (9C5), probably because the direct binding of M A1AT to the plastic plate deforms the native structure of the protein, while capturing through a single epitope better preserves the native structure of A1AT. Purified mAb 1D9 was also effective in preventing complex formation with PR3, suggesting a universal effect against the anti-protease functions of A1AT. In fact, our collaborators at the laboratory of Prof. David Lomas at UCL (UK) have confirmed a reduction in inhibitory function against chymotrypsin in enzymatic assays and found that mAb 1D9 binds A1AT at an epitope that includes part of the RCL (James Irving, personal communication). This explains the blocking activity of mAb 1D9: by binding to the RCL, it probably interferes with protease binding to its target sequence in this region of A1AT. Furthermore, the position of the 1D9 epitope also seems responsible for the decrease in polymer formation by Z A1AT in the presence of bound 1D9, since the RCL is involved in the intermolecular link necessary for polymerisation.

Although A1AT is predominantly synthesised by the liver, neutrophils, monocytes, and alveolar macrophages also express A1AT in response to a variety of inflammatory mediators (Du Bois et al., 1991, Knoell et al., 1998). A1AT has been shown to induce the production of both pro-inflammatory interleukin 1 (IL-1) and anti-inflammatory IL-1

receptor antagonist (IL-1Ra) in PBMCs (Tilg et al., 1993), and A1AT conformers (native, oxidised or polymerised forms of A1AT) act as regulators of LPS-stimulated inflammation, inhibiting the release of TNFa and IL-1b from monocytes but enhancing the release of the anti-inflammatory cytokine IL-10 (Janciauskiene et al., 2004). Starting from this information we treated the PBMCs with A1AT and our function-blocking candidate mAbs, first as hybridoma CMS and subsequently as the purified antibodies, looking at secreted IL-10 levels as our readout. Unfortunately, our results were inconclusive because the control treated with A1AT only did not show an increase in IL-10 secretion. Nevertheless, we observed that mAbs 9C5 and 1D9 caused a strong decrease in basal IL-10 secretion. These results suggest that 9C5 and 1D9 could mediate their effects by interacting directly with endogenous A1AT produced at basal levels by the PBMCs, which promotes basal IL-10 secretion from these cells. Our collaborators are currently repeating these experiments with a new batch of A1AT, in order to confirm our preliminary results, which open up the possibility of using mAbs 9C5 and 1D9 as tools to study this immunomodulatory role of A1AT.

Methods

Immunisation and isolation of spleen cells from immunised mice

These procedures were carried out by Prof. Juan Perez at the University of Malaga (Spain), as a part of a collaborative work funded by the Alpha-1 Foundation (USA). The immunisation was performed with active M A1AT purified from human plasma at 0.81 mg/ml, provided by the laboratory of Prof. David Lomas (UCL,L. Ten female mice Balb/C of 8 weeks of age were injected with the immunogen, five of the ten mice received 15 µg/dose (high dose) and the other five 7,5 µg/dose (low dose), in the first (priming) and following (booster) injections. For each dose, 140 µg M AAT were diluted to a final volume of 500 µl with PBS and emulsified with 1 ml adjuvant (Freund's complete adjuvant FCA for first dose, Freund's incomplete adjuvant FIA for boosters). Mice were injected with 100 (low dose) or 200 (high dose) µl per mouse, using a small glass syringe. Two mice died after the first dose. Spleen cells and corresponding immune sera were collected 3 days after the final injection, pooled in four aliquots [mice 1+2 (low dose), 3+4 (low dose), 5+6 (high dose) and 7+8 (high dose)], frozen, sent to our laboratory at Sapienza and kept in N_2L until fusion.

Production of hybridomas cell lines

Before fusion the spleen cells are thawed in DMEM-20 and washed with DMEM before mixing with myeloma cells. In each fusion, cells from 2 spleens (around 200 million cells)

were fused with 50 million myeloma cells P3X63Ag8.653 (X653). Cells are fused by dropwise addition of 1ml 50% (w/v) polyethylene glycol to the cell pellet at 37°C with gentle stirring. The fusion products were diluted in selective medium HAT-20 (FBS Sigma F2442) medium containing 5% of fusion cloning supplement to foster hybridoma growth (PAA Ltd, F05-009; this substituted for feeder cells) and distributed in nearly 9 plates of 96-wells at different cell densities (2 plates at 120 µl/wells, 2 plates at 60 µl/well and 6 plates at 30 µl/well). Final volume was around 200 µl per well. First clones were visible after around 4-5 days. On day 5, 50 µl/well of fresh medium were added. Afterwards, cells were fed every other day by replacing half of the volume with fresh medium. Primary screening, with the aim of identifying wells containing hybridoma colonies that produce specific antibodies, was performed at about day 8-10, after checking under the microscope that most of the colonies were big enough. Plates were fully screened when having growth in 30 or more wells, otherwise only selected wells were screened.

Antigen mediated ELISA for primary screening

General conditions for this and subsequent ELISA assays: the final volume per well is 50 µl in all the steps, except in the blocking step where is 300 µl; washes were always performed in triplicate using washing buffer (NaCl 0.9%, Tween20 0.05%).

Plates were coated with purified M A1AT, diluted at 2 µg/ml in PBS, overnight at RT (or 2 h at 37°C). After washing, the plates were blocked by adding 300 µl of blocking buffer (PBS,

BSA 0.25%, Tween 20 0.05%) and incubating for 1h at RT. After the incubation and washing the plates, we added anti-mouse-HRP secondary antibody 1:20000 for 1h 20 min RT in the dark. After developing for 10 min with TMB (Sigma), a substrate solution that HRP converts into a blue product, and the reaction terminated by adding 1M H_2SO_4, which changes the color to yellow. Color production was quantified in a Glomax plate reader (Promega) at 450 nm.

Sandwich ELISA

Plates were coated overnight with rabbit polyclonal anti A1AT antibody at 2 μg/ml in PBS overnight at RT. Next, wells were washed and blocked as above. After washing After washing, the new lines were tested, using M monomer, Z monomer and Z polymers as antigens starting from 1 μg/ml with 1:3 serial dilutions of the antigen and incubated for 1h at 37°C. Plates were washed and mAbs were added as CMS diluted to a fixed concentration: 1:100 for 2G5, 2D4 and the positive control 3C11; 1:50 for mAbs 3F7, 3G7 and 2C1, used here for comparison. Bound mAbs were detected with rabbit anti-mouse HRP antibody as above. After developing for 10 min with TMB substrate solution and stopping the reaction with 1M H_2SO_4, HRP activity was measured in a Glomax plate reader at 450 nm.

Secondary screening elastase blocking ELISA

Plates were coated with purified, active M A1AT, diluted at 2 μg/ml in PBS, overnight at 4°C. Next, wells were washed and blocked as above. Next, candidate mAbs (as CMS 1:1) were

added for 1 h 37°C, so they could bind to M A1AT. After that we added in sequence: elastase at 0.5 µg/ml for 5 min at 37°C, that formed a covalent complex with M A1AT only if the bound mAb did not interfere with binding; anti-elastase rabbit polyclonal antibody 1:2,000 for 1 h at 37°C, and anti-rabbit-HRP secondary antibody 1:15,000 for 1h 20 min at RT, with washing between each step. After developing for 10 min with TMB substrate solution and stopping the reaction with 1M H_2SO_4, HRP activity was measured in a Glomax plate reader at 450 nm. In order to improve the detection of A1AT-function-blocking antibodies, we developed an improved format for the elastase ELISA, by coating the plate with purified mAb 9C5 (an anti-A1AT polymer mAb, Miranda et al., 2010) at 4 µg/ml, which captures M A1AT by binding to its epitope. After coating with 9C5, washing, blocking and incubating with purified M A1AT at 2 µg/ml in blocking buffer for 1 h at 37°C, the rest of the assay is the same as described above.

Secondary screening proteinase 3 ELISA

Plates were coated overnight with PR3 at 10 µg/ml in PBS at 4°C. Next, wells were washed and blocked as above. In parallel, we performed a test tube incubation of M A1AT (2 µg/ml) with candidate mAbs (as CMS 1:1, 1:3 and 1:9 dilutions) for 1 h at 37°C. Next, we incubated the A1AT-mAb complexes with the PR3 in the plate for 30 min at 37°C, to promote PR3-M A1AT complex formation. After washing, anti-mouse-HRP antibody at 1:20,000 for 1h 20 min at RT. After developing for 10 min with TMB substrate solution and

stopping the reaction with 1M H_2SO_4, HRP activity was measured in a Glomax plate reader at 450 nm.

Purification of selected mAbs

We collected the CMS from overgrown hybridoma cultures and centrifuged it for ten minutes at 1,000 g, saved the CMS and discarded the pellet. The CMS was supplemented with 0.1% sodium azide to prevent contamination, filtered through a 0.45 µm filter and mixed with binding buffer (20 mM sodium phosphate, pH 7) (1V+1V) to prepare the sample for purification. We typically ran 500 ml of sample at a maximum rate of 1 ml/min with a peristaltic pump overnight at RT. After the CMS, we run binding buffer through the column until reaching the baseline (by measuring the aborbance at 280 nm). We eluted manually (using a 10-20 ml syringe connected to the column) with glycine buffer (1 M glycine-HCl, pH 2.7) and collected 1 column volume (1 ml) fractions with addition of 40 µl neutralizing buffer (1 M Tris, pH 9). Finally, the IgG concentration as measured by absorbance at 280 nm, pooled the best fractions and dialysed them against PBS overnight at 4°C.

Heat-induced polymerisation blocking test

The test for interference in the heat-driven polymerisation of Z AAT is a method that we stablished in the past to evaluate if the binding of a specific mAb to Z A1AT can modulate *in vitro* polymerisation (Ordoñez et al., 2015). Z AAT purified from human plasma was incubated with decreasing amounts (1.2, 0.5 and 0.2 mg/ml) of mAb 1D9 or the polymerisation

blocking mAb 4B12 as a reference (Ordoñez et al, 2015). We first promoted Z A1AT-mAb complex formation by incubating for 1 h at 37°C, after which heat polymerisation was induced by incubating at 45°C for 45 h. Polymer formation was quantified by sandwich ELISA by coating the plates with anti-A1AT rabbit polyclonal, followed by wash and blocking as above; incubation with the polymerisation mix diluted in blocking buffer to reach a concentration of A1AT of 3 µg/ml, for 1 h at 37°C; wash and incubation with anti-polymer mAb 2C1-HRP at 30 ng/ml in blocking buffer without sodium azide. HRP activity was developed and quantified by adding TMB and stopping the reaction with H_2SO_4 and reading the plate in the ELISA assays described above.

PBMC cultures

Human PBMCs were isolated from blood of healthy controls as follows: citrated blood was collected from volunteers and gently inverted to ensure good mixing. Citrated blood was diluted with equal quantity of Hanks' HBSS and again gently mixed. 15 ml LymphoPrep (Stem Cell Technologies), a density gradient medium for the isolation of mononuclear cells, were added into empty 50 ml Falcon tubes, and 30 ml of diluted blood were gently layered above each LymphoPrep tube using a syringe and cannula. We centrifuged the tubes at 800 g for 20 min at 4°C. Using a new 20 ml syringe and cannula, the PBMC rich fluid phase was collected from above and placed in a new 50 ml falcon tube. We centrifuged the tubes of PBMC-rich fluid at 600 g for 10 min, discarded the supernatant and resuspended the cell pellets with 1 ml 2%

FBS-HBSS per pellet, combined them in a single preparation and topped up to 50 ml with 2% FBS-HBSS. PBMCs were centrifuged at 200 g for 10 min, the supernatants were discarded, and the cell pellet resuspended with 1 ml 2% FBS-HBSS and topped up to 50 ml with 2% FBS-HBSS. Cells were counted by taking 10 µl of cell suspension and making a 1:1 dilution with Trypan blue. After taking note of the total number of cells and centrifuging again to remove the 2% FBS-HBSS used for washing, cells were resuspended in RPMI complete medium to obtain the correct number of cells for plating.

PBMCs were plated at a density of two million cells/ml. For each candidate mAb, a control well (non-treated with A1AT) and a well with A1AT at the final concentration of 125 µg/ml were prepared. 250 µl of hybridoma CMS were added to each of the experimental wells. After 24 h, the culture media and cell pellets from these PBMCs were collected for CBA analysis and Real time PCR. Our candidate mAbs were also tested as purified IgG using 187.5 µg of each purified mAb to reach an equimolecular concentration of A1AT and antibody, in triplicate wells for each mAb. After 24 h, the culture media were collected and used for IL-10 determination by CBA assay.

Cytometric bead assay (CBA) for IL-10 quantification

For the assay, standard curve cytokine standards were used consisting in 16 samples of known concentrations ranging from 50,000 pg/ml to 0.5 pg/ml. For unknown sample quantification, 50 µl of sample were incubated with 10 µl of beads coated with anti- IL-10 antibody for 3 h, after which the beads were washed in a buffer consisting in 200 ml Facs Flow (filtered, slightly buffered saline solution), 1 ml FBS, 500 µl Tween20, 100 µl 0.5M EDTA). 10 µl of anti-cytokine detection antibody were added and incubated for a further 2 h. The beads were spun down and washed, then run on a flow cytometer for quantification.

References

Aldonyte, R., Jansson, L., and Janciauskiene, S. (2004). Concentration-dependent effects of native and polymerised alpha1-antitrypsin on primary human monocytes, in vitro. BMC Cell Biol. *5*, 11.

Bergin, D.A., Reeves, E.P., Meleady, P., Henry, M., McElvaney, O.J., Carroll, T.P., Condron, C., Chotirmall, S.H., Clynes, M., O'Neill, S.J., et al. (2010). α-1 Antitrypsin regulates human neutrophil chemotaxis induced by soluble immune complexes and IL-8. J. Clin. Invest. *120*, 4236–4250.

Bergin, D.A., Reeves, E.P., Hurley, K., Wolfe, R., Jameel, R., Fitzgerald, S., and McElvaney, N.G. (2014a). The circulating proteinase inhibitor α-1 antitrypsin regulates neutrophil degranulation and autoimmunity. Sci Transl Med *6*, 217ra1.

Bergin, D.A., Reeves, E.P., Hurley, K., Wolfe, R., Jameel, R., Fitzgerald, S., and McElvaney, N.G. (2014b). The circulating proteinase inhibitor α-1 antitrypsin regulates neutrophil degranulation and autoimmunity. Sci Transl Med *6*, 217ra1.

du Bois, R.M., Bernaudin, J.F., Paakko, P., Hubbard, R., Takahashi, H., Ferrans, V., and Crystal, R.G. (1991). Human neutrophils express the alpha 1-antitrypsin gene and produce alpha 1-antitrypsin. Blood *77*, 2724–2730.

Bucurenci, N., Blake, D.R., Chidwick, K., and Winyard, P.G. (1992). Inhibition of neutrophil superoxide production by human plasma alpha 1-antitrypsin. FEBS Lett. *300*, 21–24.

Duvoix, A., Roussel, B.D., and Lomas, D.A. (2014). Molecular pathogenesis of alpha-1-antitrypsin deficiency. Rev Mal Respir *31*, 992–1002.

Eriksson, S., Carlson, J., and Velez, R. (1986). Risk of cirrhosis and primary liver cancer in alpha 1-antitrypsin deficiency. N. Engl. J. Med. *314*, 736–739.

Frenzel, E., Korenbaum, E., Hegermann, J., Ochs, M., Koepke, J., Koczulla, A.R., Welte, T., Köhnlein, T., and Janciauskiene, S. (2012). Does augmentation with alpha1-antitrypsin affect neutrophil extracellular traps formation? Int. J. Biol. Sci. *8*, 1023–1025.

Griese, M., Latzin, P., Kappler, M., Weckerle, K., Heinzlmaier, T., Bernhardt, T., and Hartl, D. (2007). alpha1-Antitrypsin inhalation reduces airway inflammation in cystic fibrosis patients. Eur. Respir. J. *29*, 240–250.

Guttman, O., Yossef, R., Freixo-Lima, G., Rider, P., Porgador, A., and Lewis, E.C. (2014). α1-Antitrypsin modifies general NK cell interactions with dendritic cells and specific interactions with islet β-cells in favor of protection from autoimmune diabetes. Immunology.

Houghton, A.M., Grisolano, J.L., Baumann, M.L., Kobayashi, D.K., Hautamaki, R.D., Nehring, L.C., Cornelius, L.A., and Shapiro, S.D. (2006). Macrophage elastase (matrix metalloproteinase-12) suppresses growth of lung metastases. Cancer Res. *66*, 6149–6155.

Hubbard, R.C., Fells, G., Gadek, J., Pacholok, S., Humes, J., and Crystal, R.G. (1991). Neutrophil accumulation in the lung in alpha 1-antitrypsin deficiency. Spontaneous release of leukotriene B4 by alveolar macrophages. J. Clin. Invest. *88*, 891–897.

Janciauskiene, S.M., Nita, I.M., and Stevens, T. (2007). Alpha1-antitrypsin, old dog, new tricks. Alpha1-antitrypsin exerts in vitro anti-inflammatory activity in human monocytes by elevating cAMP. J. Biol. Chem. *282*, 8573–8582.

Jonigk, D., Al-Omari, M., Maegel, L., Müller, M., Izykowski, N., Hong, J., Hong, K., Kim, S.-H., Dorsch, M., Mahadeva, R., et al. (2013a). Anti-inflammatory and immunomodulatory properties of α1-antitrypsin without inhibition of elastase. Proc. Natl. Acad. Sci. U.S.A. *110*, 15007–15012.

Jonigk, D., Al-Omari, M., Maegel, L., Müller, M., Izykowski, N., Hong, J., Hong, K., Kim, S.-H., Dorsch, M., Mahadeva, R., et al. (2013b). Anti-inflammatory and immunomodulatory properties of α1-antitrypsin without inhibition of elastase. Proc. Natl. Acad. Sci. U.S.A. *110*, 15007–15012.

Knoell, D.L., Ralston, D.R., Coulter, K.R., and Wewers, M.D. (1998). Alpha 1-antitrypsin and protease complexation is induced by lipopolysaccharide, interleukin-1beta, and tumor necrosis factor-alpha in monocytes. Am. J. Respir. Crit. Care Med. *157*, 246–255.

Lefrançais, E., Roga, S., Gautier, V., Gonzalez-de-Peredo, A., Monsarrat, B., Girard, J.-P., and Cayrol, C. (2012). IL-33 is

processed into mature bioactive forms by neutrophil elastase and cathepsin G. Proc. Natl. Acad. Sci. U.S.A. *109*, 1673–1678.

Lockett, A.D., Kimani, S., Ddungu, G., Wrenger, S., Tuder, R.M., Janciauskiene, S.M., and Petrache, I. (2013). α_1-Antitrypsin modulates lung endothelial cell inflammatory responses to TNF-α. Am. J. Respir. Cell Mol. Biol. *49*, 143–150.

Lomas, D.A., Evans, D.L., Finch, J.T., and Carrell, R.W. (1992). The mechanism of Z alpha 1-antitrypsin accumulation in the liver. Nature *357*, 605–607.

Mahadeva, R., Atkinson, C., Li, Z., Stewart, S., Janciauskiene, S., Kelley, D.G., Parmar, J., Pitman, R., Shapiro, S.D., and Lomas, D.A. (2005). Polymers of Z alpha1-antitrypsin co-localize with neutrophils in emphysematous alveoli and are chemotactic in vivo. Am. J. Pathol. *166*, 377–386.

Marcondes, A.M., Li, X., Tabellini, L., Bartenstein, M., Kabacka, J., Sale, G.E., Hansen, J.A., Dinarello, C.A., and Deeg, H.J. (2011). Inhibition of IL-32 activation by α-1 antitrypsin suppresses alloreactivity and increases survival in an allogeneic murine marrow transplantation model. Blood *118*, 5031–5039.

Marcondes, A.M., Karoopongse, E., Lesnikova, M., Margineantu, D., Welte, T., Dinarello, C.A., Hockenbery, D., Janciauskiene, S., and Deeg, H.J. (2014a). α-1-Antitrypsin (AAT)-modified donor cells suppress GVHD but enhance the

GVL effect: a role for mitochondrial bioenergetics. Blood *124*, 2881–2891.

Marcondes, A.M., Karoopongse, E., Lesnikova, M., Margineantu, D., Welte, T., Dinarello, C.A., Hockenbery, D., Janciauskiene, S., and Deeg, H.J. (2014b). α-1-Antitrypsin (AAT)-modified donor cells suppress GVHD but enhance the GVL effect: a role for mitochondrial bioenergetics. Blood *124*, 2881–2891.

Miranda, E., Pérez, J., Ekeowa, U.I., Hadzic, N., Kalsheker, N., Gooptu, B., Portmann, B., Belorgey, D., Hill, M., Chambers, S., et al. (2010). A novel monoclonal antibody to characterize pathogenic polymers in liver disease associated with alpha1-antitrypsin deficiency. Hepatology *52*, 1078–1088.

Morris, H., Morgan, M.D., Wood, A.M., Smith, S.W., Ekeowa, U.I., Herrmann, K., Holle, J.U., Guillevin, L., Lomas, D.A., Perez, J., et al. (2011). ANCA-associated vasculitis is linked to carriage of the Z allele of α_1 antitrypsin and its polymers. Ann. Rheum. Dis. *70*, 1851–1856.

Nita, I., Hollander, C., Westin, U., and Janciauskiene, S.-M. (2005). Prolastin, a pharmaceutical preparation of purified human alpha1-antitrypsin, blocks endotoxin-mediated cytokine release. Respir. Res. *6*, 12.

Ordóñez, A., Pérez, J., Tan, L., Dickens, J.A., Motamedi-Shad, N., Irving, J.A., Haq, I., Ekeowa, U., Marciniak, S.J., Miranda, E., et al. (2015). A single-chain variable fragment

intrabody prevents intracellular polymerisation of Z α1-antitrypsin while allowing its antiproteinase activity. FASEB J. *29*, 2667–2678.

Senior, R.M., Griffin, G.L., and Mecham, R.P. (1980). Chemotactic activity of elastin-derived peptides. J. Clin. Invest. *66*, 859–862.

Shahaf, G., Moser, H., Ozeri, E., Mizrahi, M., Abecassis, A., and Lewis, E.C. (2011). α-1-antitrypsin gene delivery reduces inflammation, increases T-regulatory cell population size and prevents islet allograft rejection. Mol. Med. *17*, 1000–1011.

Sinden, N.J., and Stockley, R.A. (2013). Proteinase 3 activity in sputum from subjects with alpha-1-antitrypsin deficiency and COPD. Eur. Respir. J. *41*, 1042–1050.

Sinden, N.J., Baker, M.J., Smith, D.J., Kreft, J.-U., Dafforn, T.R., and Stockley, R.A. (2015). α-1-antitrypsin variants and the proteinase/antiproteinase imbalance in chronic obstructive pulmonary disease. Am. J. Physiol. Lung Cell Mol. Physiol. *308*, L179-190.

Subramaniyam, D., Steele, C., Köhnlein, T., Welte, T., Grip, O., Matalon, S., and Janciauskiene, S. (2010). Effects of alpha 1-antitrypsin on endotoxin-induced lung inflammation in vivo. Inflamm. Res. *59*, 571–578.

Surmiak, M., and Sanak, M. (2016). Different forms of alpha-1 antitrypsin and neutrophil activation mediated by human anti-PR3 IgG antibodies. Pharmacol Rep *68*, 1276–1284.

Suzuki, T., Moraes, T.J., Vachon, E., Ginzberg, H.H., Huang, T.-T., Matthay, M.A., Hollenberg, M.D., Marshall, J., McCulloch, C.A.G., Abreu, M.T.H., et al. (2005). Proteinase-activated receptor-1 mediates elastase-induced apoptosis of human lung epithelial cells. Am. J. Respir. Cell Mol. Biol. *33*, 231–247.

Suzuki, T., Yamashita, C., Zemans, R.L., Briones, N., Van Linden, A., and Downey, G.P. (2009). Leukocyte elastase induces lung epithelial apoptosis via a PAR-1-, NF-kappaB-, and p53-dependent pathway. Am. J. Respir. Cell Mol. Biol. *41*, 742–755.

Sveger, T. (1976). Liver disease in alpha1-antitrypsin deficiency detected by screening of 200,000 infants. N. Engl. J. Med. *294*, 1316–1321.

Taipale, J., Lohi, J., Saarinen, J., Kovanen, P.T., and Keski-Oja, J. (1995). Human mast cell chymase and leukocyte elastase release latent transforming growth factor-beta 1 from the extracellular matrix of cultured human epithelial and endothelial cells. J. Biol. Chem. *270*, 4689–4696.

Tan, L., Perez, J., Mela, M., Miranda, E., Burling, K.A., Rouhani, F.N., DeMeo, D.L., Haq, I., Irving, J.A., Ordóñez, A., et al. (2015). Characterising the association of latency with α (1)-antitrypsin polymerisation using a novel monoclonal antibody. Int. J. Biochem. Cell Biol. *58*, 81–91.

Tilg, H., Vogel, W., Wiedermann, C.J., Shapiro, L., Herold, M., Judmaier, G., and Dinarello, C.A. (1993). Circulating interleukin-1 and tumor necrosis factor antagonists in liver disease. Hepatology *18*, 1132–1138.

Van ’t Wout, E.F.A., Dickens, J.A., van Schadewijk, A., Haq, I., Kwok, H.F., Ordóñez, A., Murphy, G., Stolk, J., Lomas, D.A., Hiemstra, P.S., et al. (2014). Increased ERK signalling promotes inflammatory signalling in primary airway epithelial cells expressing Z α1-antitrypsin. Hum. Mol. Genet. *23*, 929–941.

GENERAL CONCLUSIONS AND FUTURE PERSPECTIVES

In conclusion, in the first part of this work we show for the first time that expression of a strongly polymerogenic variant of neuroserpin that causes severe neurodegeneration FENIB leads to morphological and functional alterations in the mitochondrial network of cells differentiated to neurons. These deregulations can be exacerbated by removal of antioxidant defenses, which we have shown to be upregulated in cells expressing mutant polymerogenic NS, but also rescued with antioxidant molecules. This is in line with our previous work showing, in the same cell model system, that expression of G392E NS caused oxidative stress in these cells. Our studies support that mitochondrial alterations and oxidative stress are thus part of the toxicity exerted by neuroserpin polymers in FENIB, adding this type of neurodegeneration to the increasing list where such alterations have been involved in neuronal death. Surely, there are other players involved in the oxidative stress pathway as well as aspects of mitochondrial dynamics and physiology that we have not considered yet. To further investigate these aspects, one of our future goals is to investigate calcium signaling to evaluate possible changes in flux between ER and mitochondria, to better understand the signaling at MAMs that seems to be disrupted in our system. Finally, in view of the changes we have found in cell morphology in association with the actin cytoskeleton, it would be also interesting to investigate the consequences that the accumulation of NS polymers has on cytoskeletal dynamics in neurons, and to look at its influence

in mitochondrial dynamics and neuronal trafficking with a live imaging approach.

In the second part of this work we have developed new tools to investigate the mechanisms of immunomodulatory roles of A1AT in health and disease. We have produced specific monoclonal antibodies against the native form of M A1AT that may be useful in future studies in this field. By using novel screening methods set up for this work, we have also identified mAb 1D9 as able to reduce complex formation with both elastase and proteinase 3, two of its main physiological targets. This mAb is also able to block the heat-induced polymerisation of Z A1AT and, together with mAb 9C5, to modulate IL-10 secretion in PBMCs. The position of the 1D9 mAb epitope, partially covering the RCL, is congruent with many of these activities, which render mAb 1D9 a useful tool to study A1AT physiological functions and pathological polymer formation. 1D9 is also under investigation at the laboratory of Prof. David Lomas at UCL, where purified 1D9 has been shown to block the inhibitory activity of A1AT against chymotrypsin and elastase in enzymatic assays and its epitope has been described by crystallographic studies. Current work at Prof. Hawrylowicz's laboratory at King's College London is being conducted to reproduce our results with 1D9 and 9C5 on PBMC cultures with a valid A1AT positive control. If successful, this will be the first report showing inhibition of an immunomodulatory role of A1AT by a mAb *in vitro*, opening a new direction in the field. Further investigation into the mechanism through which 1D9 and 9C5 decrease IL-10 secretion can lead to the identification of the domain in A1AT responsible for this particular function.

AWARDS AND GRANTS

- January 2020 Awarded NeuroSpritz travel grant for young Researchers

- October 2019 Awarded one-year research fellow "Characterization of mitochondrial alterations in a neuronal model of dementia FENIB"

- October 2019 Awarded grant from Sapienza University of Rome for assistance in the course of cellular biology

- May 2019 Awarded travel grant for SINS annual meeting

- November 2018 Awarded grant from Sapienza University of Rome "PLS, Piano Lauree Scientifiche", Assistance in the course of cellular biology

- November 2017 Awarded grant from Sapienza University of Rome "PLS, Piano Lauree Scientifiche", Assistance in the course of cellular biology

- July 2017: Grant from Sapienza University of Rome "Avvio alla Ricerca": "Characterization of mitochondrial alterations in a model of dementia FENIB"

- November 2016: Awarded grant from Sapienza University of Rome "PLS, Piano Lauree Scientifiche", Assistance in the course of cellular biology

- September 2016: Awarded a PhD fellowship in Cellular and Developmental Biology

- September 2016: Awarded a PhD fellowship in experimental clinical neuroscience and psychiatry

STAGES

- June 6th - August 15th, 2019 Intership at University Medical Centre of Hamburg- Eppendorf for the project: "Mutant Neuroserpin induces mitochondrial alterations in a neuronal model of neurodegeneration FENIB"

- July 2nd - August 1st, 2018 Intership at King's College London for the project "Dissecting immunomodulatories roles of A1AT with function-neutralising monoclonal antibodies"

CONFERENCE ORAL PRESENTATIONS

D'Acunto E, Cheadle C, Elliston ELK, Laffranchi M, Heyer-Chauhan N, Irving JA, Lomas DA, Gooptu B, Hawrylowicz CM, Perez J, Miranda E. "Developing function-blocking monoclonal antibodies against alpha1-antitrypsin to understand its immunomodulatory functions". Molecular therapies for liver disease in alpha1 antitrypsin deficiencyAATD2019 TIGEM, Pozzuoli, Italy, September 2019.

D'Acunto E, Gianfrancesco L, D'Orsi M, Guadagno NA, Bhosale G, Cacci E, Lupo G, Duchen MR, Galliciotti G,

Miranda E. “Mutant neuroserpin induces mitochondrial alterations in a neuronal model of neurodegeneration FENIB”, SINS congress, Perugia, Italy, September 2019

CONFERENCE COMMUNICATIONS

D’Acunto E, Gianfrancesco L, D’Orsi M, Guadagno NA, Bhosale G, Cacci E, Lupo G, Duchen MR, Galliciotti G, Miranda E. “Mutant neuroserpin induces mitochondrial alterations in a neuronal model of neurodegeneration FENIB”, International Symposium on serpins and proteases in health and disease, Seville, Spain, September 2019

D’Acunto E, Gianfrancesco L, D’Orsi M, Guadagno NA, Bhosale G, Cacci E, Lupo G, Duchen MR, Galliciotti G, Miranda E. “Mutant neuroserpin induces mitochondrial alterations in a neuronal model of neurodegeneration FENIB”, SINS congress, Perugia, Italy, September 2019

Laffranchi M, Perez J, Elliston ELK, **D’Acunto E**, Heyer-Chauhan N, Cheadle C, Hawrylowicz CM, Gooptu B, Fra AM, Lomas DA, Irving JA, Miranda E. “Conformational-specific monoclonal antibodies against alpha1-antitrypsin to investigate its physiological and pathological roles”, International Symposium on serpins and proteases in health and disease, Seville, Spain, September 2019

D’Acunto E, Cheadle C, Elliston ELK, Laffranchi M, Heyer-Chauhan N, Irving JA, Lomas DA, Gooptu B, Hawrylowicz CM, Perez J, Miranda E. “Developing function-blocking monoclonal antibodies against alpha1-antitrypsin to

understand its immunomodulatory functions". AATD2019 TIGEM, Pozzuoli, Italy, September 2019.

D'Acunto E, Gianfrancesco L, D'Orsi M, Guadagno NA, Bhosale G, Cacci E, Lupo G, Duchen MR, Galliciotti G, Miranda E."Mutant neuroserpin induces mitochondrial alterations in a neuronal model of neurodegeneration FENIB", GEI 2019, Ancona, Italy, July 2019.

D'Acunto E, Cheadle C, Gooptu B, Hawrylowicz CM, Perez J, Miranda E. "Developing functional-blocking monoclonal antibodies against alpha 1 antitrypsin to understand its immunomodulatory functions" – Alpha 1 Foundation annual investigator's meeting 2018, Miami, California, USA.

Guadagno NA, Moriconi C, Licursi V, **D'Acunto E**, Nisi PS, Carucci N, De Jaco A, Cacci E, Negri R, Lupo G, Miranda E. "Neuroserpin polymers cause oxidative stress in a neuronal model of the dementia FENIB." - The 8th International Symposium on Serpins and Proteases in Health and Disease, Shaghai, China.

Guadagno NA, Moriconi C, Licursi V, **D'Acunto E**, Nisi PS, Carucci N, De Jaco A, Cacci E, Negri R, Lupo G, Miranda E. "Neuroserpin polymers cause oxidative stress in a neuronal model of the dementia FENIB." - 63° GEI- Embriologic Italian Group, Rome, Italy.

LIST OF PUBLICATIONS

Guadagno NA, Moriconi C, Licursi V, **D'Acunto E**, Nisi PS, Carucci N, De Jaco A, Cacci E, Negri R, Lupo G, Miranda E. "Neuroserpin polymers cause oxidative stress in a neuronal model of the dementia FENIB." *Neurobiol Dis*. 2017 Jul; 103:32-44

Piscopo P, Grasso M, Puopolo M, **D'Acunto E**, Talarico G, Crestini A, Gasparini M, Campopiano R, Gambardella S, Castellano AE, Bruno G, Denti MA, Confaloni AM. "Circulating miR-127-3p as a Potential Biomarker for Differential Diagnosis in Frontotemporal Dementia." Journal of Alzheimer's Disease. 2018 Jun; 10.3233/JAD-180364

Fra A, **D'Acunto E**, Laffranchi M, Miranda E. "Cellular Models for the Serpinopathies" Book Chapter "Serpins: Methods and Protocols", Methods in Molecular Biology, vol.1826, 2018 Sept.

Galliciotti G, De Jaco A, Sepulveda-Falla D, **D'Acunto E**, Miranda E, "Role of cellular oxidative stress in dementia" Book Chapter *in press*

Ringraziamenti

Grazie ad Elena, che mi ha insegnato il rigore, la costanza e soprattutto l'entusiasmo per la scienza

Grazie a Giovanna, che mi ha accolta nella terra delle Eppendorf, con un affetto ed una generosità che conservo nel cuore

Grazie a Paola, che mi ha fatto il più bello dei regali, la sua amicizia incondizionata sempre, comunque, dovunque

Grazie a Laura, che ho imparato con calma e curiosità a voler bene

Grazie a Lorita, che mi ha fatto scoprire una delle cose più stupefacenti, che si può imparare insegnando

Grazie a Beatrice e Valeria, fantastiche compagne di viaggio, di risate e aperitivi

Grazie a Sara, un pozzo inesauribile di sorrisi, sostegno e comprensione

Grazie a Gabriele, le cui braccia mi hanno rialzata quando ero scoraggiata, confortata quando ho cercato rifugio, spinta in avanti quando avevo bisogno di coraggio

Grazie alla Ricerca, che mi ha insegnato a convivere ed accettare le mie sconfitte con serenità, a passare una spugna sul giorno passato e ricominciare quello seguente, ad affidarmi a me stessa più di quanto avrei mai sperato di poter fare.

Ed infine grazie a me, che in fin dei conti, nonostante tutto, ce l'ho fatta.